Journal of Non-Crystalline Solids 450 (2016) 194–208

Contents lists available at ScienceDirect

Journal of Non-Crystalline Solids

journal homepage: www.elsevier.com/locate/jnoncrysol

Renormalization approach to the electronic localization and transport in macroscopic generalized Fibonacci lattices

Fernando Sánchez [a], Vicenta Sánchez [a], Chumin Wang [b,*]

[a] Departamento de Física, Facultad de Ciencias, Universidad Nacional Autónoma de México, Mexico City, Mexico
[b] Instituto de Investigaciones en Materiales, Universidad Nacional Autónoma de México, Mexico City, Mexico

ARTICLE INFO

Article history:
Received 22 April 2016
Received in revised form 16 July 2016
Accepted 23 July 2016

Keywords:
Kubo-Greenwood formula
Real-space renormalization method
Generalized Fibonacci lattices

ABSTRACT

Electronic transport and wavefunction localization are two closely related phenomena, but their behavior in truly macroscopic aperiodic lattices is a non-widely addressed issue. We study in this article the electrical conductivity of generalized Fibonacci (GF) lattices through the Kubo-Greenwood formula, while the localization of electronic wavefunction is analyzed by means of the Lyapunov exponent and participation ratio (*PR*). For periodic chains, an analytical expression of the Lyapunov exponent is obtained. We have also developed for the first time a real-space renormalization method to calculate the *PR* of macroscopic GF lattices described by tight-binding Hamiltonians. Moreover, we report a novel unified renormalization method for the Kubo-Greenwood formula applied to GF chains. For quasiperiodic lattices, the results reveal a power-law decay of the spectral averages for both *PR* and DC conductivity when the system length increases. In addition, we present a systematic analysis of the AC conductivity spectra observing truly large resonant peaks in comparison to the ballistic one. The electrical conductance of GF nanowires is also investigated. Finally, the results suggest that *PR* could not be proper for the analysis of critically localized states.

1. Introduction

The structural disorder of a solid can profoundly modify the nature of electronic states. It is well known that they are all extended in periodic lattices and exponentially localized in random-disordered systems of one and two dimensions [1]. However, the degree of localization in other non-periodic systems is still an unclear subject. In fact, delocalized electronic states are found in one-dimensional systems with correlated disorder [2,3] and some of these results have been experimentally confirmed [4,5].

Nowadays, the study of electronic states in artificial structures is of great importance in condensed matter physics, because they introduce many new physical properties essential for technological applications of atomic-scale devices. These structures can be multilayers, quantum wires, rings, or dots, etc. In particular, quasiperiodic and aperiodic systems become a subject of remarkable interest since the discovery of quasicrystals [6] and the fabrication of high-quality superlattices including quasiperiodic ones [7], whose Raman spectrum has a good agreement with the theory [8]. Much attention has been devoted to the Fibonacci lattice, because it provides a prototype structure for studying quasiperiodic systems and possesses critically localized electronic states [9]. The corresponding energy spectrum is neither absolutely continuous nor pure point, but singular continuous [10].

There is a generalization of the Fibonacci sequence obtained by the substitutions $A \to A^m B^n$ and $B \to A$, where m and n are positive integer numbers. The symbol A^m represents a string of m A's. The original Fibonacci sequence is recovered when $m = n = 1$ and generalized ones with $m > 1$ and $n = 1$ are called precious means, while metallic means stand for sequences with $m = 1$ and $n > 1$ [11]. Along last two decades, the electronic, vibrational, and optical properties of generalized Fibonacci (GF) lattices have been investigated [11–14]. In particular, real-space renormalization-group methods based on the decimation technique were developed for calculating the local density of states at any given site [15] and the average Green's functions [16] of several macroscopic GF lattices. Moreover, the total density of states and the electrical conductivity in mixing Fibonacci chains with $m = n = 1$ are investigated [17], and the alternating current (AC) of transparent states is also analyzed [18] observing a decreasing oscillatory behavior as occurred in periodic lattices, in contrast to the resonant AC conduction found at bandgap energies [19].

In this article, we report a detailed analysis of the electrical conductivity, Lyapunov coefficient, and participation ratio (*PR*) of GF lattices with macroscopic length. This analysis was carried out by means of a real-space renormalization method capable to address truly macroscopic systems without introducing any additional approximations, whose mathematical formulations are presented in Appendices *A*, *B* and *C*. We will introduce the GF sequences in section two, and define the localization and transport physical quantities in section three. The results of both direct current (DC) conductivity and the wavefunction localization

* Corresponding author.
E-mail address: chumin@unam.mx (C. Wang).

http://dx.doi.org/10.1016/j.jnoncrysol.2016.07.031
0022-3093/

are presented in section four, while the AC conduction is investigated in section five. We further discuss the electronic transport and localization in GF nanowires with a square cross-section in section six. Finally, the conclusions of this study are given in section seven.

2. Generalized Fibonacci sequences

The Fibonacci chains can be studied in several forms, for example, by using two sorts of bonds (bond problem), two kinds of atoms (site problem) or a combination of both (mixing problem) [17]. In this paper, we analyze the bond problem, in which two hoping integrals, t_A and t_B, are arranged following the GF sequences and the nature of atoms are assumed to be the same with a null self-energy. The GF sequences (S_l) can be built by using the following addition scheme [13,20],

$$\begin{aligned} &S_0(m,n)=\{B\},\ \ S_1(m,n)=\{A\},\\ &\text{and}\ \ S_l(m,n)=S_{l-1}^{m}(m,n)\oplus S_{l-2}^{n}(m,n), \end{aligned} \tag{1}$$

where l is the generation index, m and n are positive integers that define the type (m,n) of GF sequences. For example, $S_2(2,1)=\{AAB\}$ and $S_3(2,1)=\{AABAABA\}$. These $S_l(m,n)$ can also be obtained by the substitution rules given by [20,21]

$$A\rightarrow A^{m}B^{n}\ \ \text{and}\ \ B\rightarrow A, \tag{2}$$

which may be rewritten by using the substitution matrix ($\mathbf{M}$) as [22]

$$\begin{aligned} \begin{pmatrix} A\\ B \end{pmatrix}\rightarrow \boldsymbol{M}\begin{pmatrix} A\\ B \end{pmatrix}&=\begin{pmatrix} m & n\\ 1 & 0 \end{pmatrix}\begin{pmatrix} A\\ B \end{pmatrix}\\ &=\begin{pmatrix} \underbrace{AA\cdots A}_{m} & \underbrace{BB\cdots B}_{n}\\ A & \end{pmatrix}. \end{aligned} \tag{3}$$

Matrix $\mathbf{M}$ has the following eigenvalues ($\lambda_{\pm}$),

$$\begin{aligned} \begin{vmatrix} m-\lambda & n\\ 1 & -\lambda \end{vmatrix}=0 \qquad &\Rightarrow \lambda^2-m\lambda-n=0\\ \Rightarrow\ \lambda_{\pm}&=\frac{m\pm\sqrt{m^2+4n}}{2}. \end{aligned} \tag{4}$$

For $n=1$, Eq. (4) leads to $\lambda_{+}>1$ and $|\lambda_{-}|<1$, which fulfill the Pisot condition [22,23].

Moreover, the determinant of $\mathbf{M}$,

$$\begin{vmatrix} m & n\\ 1 & 0 \end{vmatrix}=-n, \tag{5}$$

is unimodular if $n=1$. Hence, the corresponding sequence is called quasiperiodic and possesses Bragg-peak diffraction spectra, because both the Pisot eigenvalue condition and the unit-determinant requirement of $\mathbf{M}$ are satisfied [24]. Conversely, the GF sequences with $n\neq 1$ do not satisfy the Pisot condition neither the unit-determinant requirement, thus they are not quasiperiodic. Among non-quasiperiodic structures, the Thue-Morse sequence is another widely studied one, since it accomplishes the Pisot condition but has a non-unimodular substitution matrix; in consequence, it is not quasiperiodic neither [25].

The total number of A and B in $S_l(m,n)$, denoted by $F_l(m,n)$, satisfies the relation

$$F_l(m,n)=mF_{l-1}(m,n)+nF_{l-2}(m,n) \tag{6}$$

with $F_0(m,n)=F_1(m,n)=1$. At the limit of infinite length, the ratio of $F_l(m,n)$ for subsequent generations defined as

$$\tau(m,n)\equiv\lim_{l\to\infty}\frac{F_{l+1}(m,n)}{F_l(m,n)} \tag{7}$$

satisfies the quadratic equation $\tau^2-m\tau-n=0$, whose positive solution is

$$\tau(m,n)=\frac{m+\sqrt{m^2+4n}}{2}. \tag{8}$$

In fact, the irrational number $\tau(1,1)=(1+\sqrt{5})/2$ is referred as the golden mean, $\tau(2,1)=1+\sqrt{2}$ as the silver mean, $\tau(3,1)=(3+\sqrt{13})/2$ as the bronze mean, $\tau(1,2)=2$ as the copper mean, and $\tau(1,3)=(1+\sqrt{13})/2$ as the nickel mean.

Both substitution and addition methods for the nine GF sequences, with m and $n=1$, 2 or 3, analyzed in this paper are summarized in Table 1. Segments of these GF chains for the bond problem are illustrated in Fig. 1, where the initial conditions were $S_0(m,n)=\{B\}$ and $S_1(m,n)=\{A\}$. Notice that for a given generation l, a GF chain of type (3,3) has more atoms than a standard Fibonacci chain with (1,1).

In the next section, we describe the model used for the study of electronic transport and localization of wavefunctions in GF chains defined in this section.

3. Modeling electronic transport and localization

In order to isolate the quasicrystalline effects on the physical properties of GF chains, let us consider a single-band tight-binding Hamiltonian (H) given by

$$H=\sum_{<i,j>}t_{i,j}\{|i><j|+|j><i|\}, \tag{9}$$

where $|j\rangle$ represents the Wannier function of atom j with null self-energy and $t_{i,j}$ is the hopping integral between nearest-neighbor sites i and j, indicated by $\langle i,j\rangle$, which may be t_A or t_B arranged according to the GF sequences.

The density of states (DOS) can be calculated by means of the retarded single-electron Green's function (G) [26],

$$DOS(E)=-\frac{1}{\pi}\lim_{\eta\to 0^{+}}\mathrm{Im}Tr[G(E+i\eta)], \tag{10}$$

where η is the imaginary part of energy (E) and the Green's function is determined by the Dyson equation given by $(E-H)G=1$.

The electronic wavefunction ($|\psi>=\sum_j c_j|j>$) satisfies the stationary Schrödinger's equation, which for both periodic or non-periodic chains described by Hamiltonian (Eq. (9)) can be written as

$$\boldsymbol{C}_{j+1}=\boldsymbol{T}_j\boldsymbol{C}_j, \tag{11}$$

where

$$\begin{aligned} \boldsymbol{T}_j&=\begin{pmatrix} E/t_{j,j+1} & -t_{j,j-1}/t_{j,j+1}\\ 1 & 0 \end{pmatrix}\\ &\text{and}\ \ \boldsymbol{C}_j=\begin{pmatrix} c_j\\ c_{j-1} \end{pmatrix} \end{aligned} \tag{12}$$

are respectively the transfer matrix and amplitude vector of the wavefunction. The amplitude vectors of atoms at the begin and end of the chain are related by the product of transfer matrices,

$$\boldsymbol{T}_N\boldsymbol{T}(l)\boldsymbol{T}_1\equiv\boldsymbol{T}_N\left(\prod_{j=2}^{N-1}\boldsymbol{T}_j\right)\boldsymbol{T}_1=\begin{pmatrix} \tau_{11} & \tau_{12}\\ \tau_{21} & \tau_{22} \end{pmatrix}, \tag{13}$$

where N is the number of atoms in the chain of generation l,

$$\boldsymbol{T}(l)=\prod_{j=2}^{N-1}\boldsymbol{T}_j, \tag{14}$$

Table 1
Substitution and addition rules for the GF sequences of type (m, n).

	n = 1	n = 2	n = 3
m = 1	$A\to AB$ & $B\to A$ $S_l = S_{l-1}\oplus S_{l-2}$	$A\to ABB$ & $B\to A$ $S_l = S_{l-1}\oplus 2S_{l-2}$	$A\to ABBB$ & $B\to A$ $S_l = S_{l-1}\oplus 3S_{l-2}$
m = 2	$A\to AAB$ & $B\to A$ $S_l = 2S_{l-1}\oplus S_{l-2}$	$A\to AABB$ & $B\to A$ $S_l = 2S_{l-1}\oplus 2S_{l-2}$	$A\to AABBB$ & $B\to A$ $S_l = 2S_{l-1}\oplus 3S_{l-2}$
m = 3	$A\to AAAB$ & $B\to A$ $S_l = 3S_{l-1}\oplus S_{l-2}$	$A\to AAABB$ & $B\to A$ $S_l = 3S_{l-1}\oplus 2S_{l-2}$	$A\to AAABBB$ & $B\to A$ $S_l = 3S_{l-1}\oplus 3S_{l-2}$

and the transfer matrices that connect the system to the semi-infinite periodic leads with null self-energies and hopping integrals t are

$$\boldsymbol{T}_1 = \begin{pmatrix} E/t_{1,2} & -t/t_{1,2} \\ 1 & 0 \end{pmatrix} \quad \text{and} \quad \boldsymbol{T}_N = \begin{pmatrix} E/t & -t_{N-1,N}/t \\ 1 & 0 \end{pmatrix}. \tag{15}$$

From Eq. (13), the transmittance (T) of a linear chain is given by [27]

$$T(E) = \frac{4-\left(\frac{E}{t}\right)^2}{\left[\tau_{21}-\tau_{12}+\frac{(\tau_{22}-\tau_{11})E}{2t}\right]^2 + (\tau_{22}+\tau_{11})^2\left(1-\frac{E^2}{4t^2}\right)}. \tag{16}$$

The electrical conductance (g) can be calculated through the Landauer formula [28]

$$\mathrm{g}(E) = \frac{2e^2}{h}T(E) = \mathrm{g}_0 T(E), \tag{17}$$

where $\mathrm{g}_0 \equiv 2e^2/h$ is the quantum of conductance.

The localization of wavefunction can be analyzed by looking at the Lyapunov coefficient (γ) and the participation ratio (PR), which are respectively defined by [27]

$$\gamma(E) = \frac{1}{N}\ln\sqrt{\tau_{1,1}^2+\tau_{1,2}^2+\tau_{2,1}^2+\tau_{2,2}^2} \quad \text{and} \quad PR(E) = \left(\sum_{j=1}^{N}|c_j(E)|^4\right)^{-1}. \tag{18}$$

In general, the inverse of γ is interpreted as the localization length if the wavefunction is exponentially localized. On the other hand, PR counts the number of atoms that contributes to a normalized wavefunction, *e.g.*, $PR = N$ for a fully extended state and $PR = 1$ for a wavefunction with amplitude only at a single atom.

Within the linear response theory, the electrical conductivity can be calculated by means of the Kubo-Greenwood formula [29],

$$\sigma(\mu,\omega,T) = \frac{2e^2\hbar}{\Omega\pi m^2}\int_{-\infty}^{\infty} \mathrm{d}E \frac{f(E)-f(E+\hbar\omega)}{\hbar\omega} \times \mathrm{Tr}\left[p\ \mathrm{Im}G^+(E+\hbar\omega)\ p\ \mathrm{Im}G^+(E)\right], \tag{19}$$

where Ω is the system volume, $p = \frac{im}{\hbar}[H,x] = \sum_j\{t_{j,j+1}|j><j+1| - t_{j,j-1}|j><j-1|\}$ is the projection of the momentum operator along the applied electrical field, $G^+(E) = G(E+i\eta)$ is the retarded one-particle Green's function, and $f(E) = \{1+\exp[(E-\mu)/k_BT]\}^{-1}$ is the Fermi-Dirac distribution with the chemical potential μ and temperature T.

For a periodic linear chain of N atoms with null self-energies and hopping integral t, connected to two semi-infinite periodic leads with the same t, the AC conductivity at zero temperature has an analytical solution of [30]

$$\sigma_P(\mu,\omega,0) = \frac{8e^2t^2a}{\pi(N-1)\hbar^3\omega^2}\left[1-\left(\frac{\mu}{2t}\right)^2\right] \times \left\{1-\cos\left[\frac{(N-1)\hbar\omega}{2t\sqrt{1-(\mu/2t)^2}}\right]\right\}, \tag{20}$$

when $-2|t| \le \mu \le 2|t|$. In particular, its DC conductivity for $\omega \to 0$ is

$$\sigma_P \equiv \sigma_P(\mu,0,0) = \frac{e^2a}{\pi\hbar}(N-1). \tag{21}$$

It is easy to verify that $\sigma_P(\mu,\omega,0) \le \sigma_P$ for $-2|t| \le \mu \le 2|t|$. Analytical solutions can also be found for the density of states $DOS(E) = N(\pi\sqrt{4t^2-E^2})^{-1}$, the participation ratio $PR(E) = N$ and the Lyapunov coefficient

$$\gamma_p(E) = \frac{1}{2N}\ln\left\{2+\frac{E^2}{t^2}\left[f(N-1)+2\sum_{i=0}^{N-2}f(i)\right]\right\} \tag{22}$$

where

$$f(J) = \sum_{l=0}^{\lfloor J/2\rfloor}\frac{(-1)^l(J-l)!}{l!(J-2l)!}\left(\frac{E^2}{t^2}-2\right)^{J-2l}. \tag{23}$$

However, there are no general analytical solutions for these physical quantities in long GF chains and they are calculated in this article by means of the real-space renormalization method, whose procedure can be illustrated for the case of transfer matrix, by using the method of addition given by Eq. (1) and by taking the advantage of the associativity of matrix products. For example, the transfer matrix of a (m,n)-type GF chain of generation l can be calculated by

$$\boldsymbol{T}(l) = [\boldsymbol{T}(l-2)]^n\boldsymbol{T}_M[\boldsymbol{T}(l-1)]^m, \tag{24}$$

where the middle connecting matrix ($\boldsymbol{T}_M$) is given by

$$\boldsymbol{T}_M = \begin{pmatrix} E/t_A & -t_M/t_A \\ 1 & 0 \end{pmatrix} \tag{25}$$

being $t_M = t_A$ if l is odd and $t_M = t_B$ if l is even. In other words, the transfer matrix of generation l can be obtained just by multiplying n times the transfer matrix of generation $l-2$ and m times the transfer matrix of generation $l-1$. Nevertheless, the formulation of this renormalization procedure for the DOS and PR is considerably more complex, whose mathematical details are respectively given in Appendices A and B. It is worth mentioning that once these new renormalization methods are developed, the computing time is proportional to the generation number l, *i.e.*, it is proportional to the logarithm of the system length.

In the next section, we present the results of DOS, DC conductivity, Lyapunov coefficient, and participation ratio for the nine GF chains of type (m,n) with m and n equal to 1, 2, or 3.

4. Localization and DC conductivity

In order to study macroscopic GF chains with lengths of 10^8 atoms, different generation numbers (l) are chosen for each type of GF chains, as specified in Table 2.

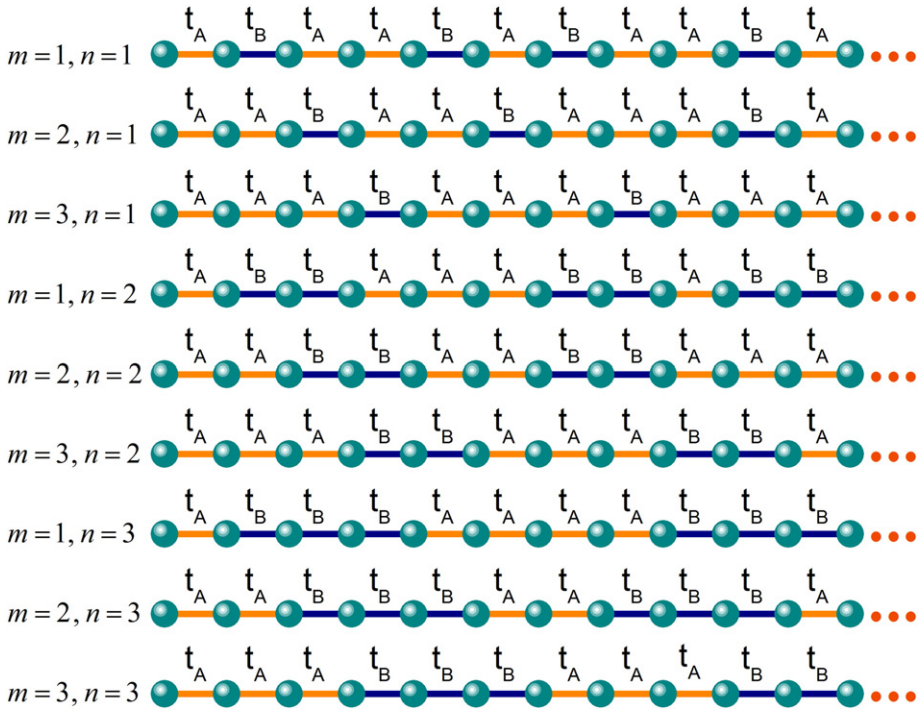

Fig. 1. Segments of generalized Fibonacci chains of type (m,n) defined by Eq. (2) for the bond problem with m and n equal to 1, 2, or 3. Two hopping strengths of bonds, t_A and t_B, are indicated.

For the sake of simplicity, a uniform bond length (a) is taken and the aperiodicity is introduced through the order of hopping integrals t_A and t_B. Two semi-infinite periodic leads with null self-energy and hopping integral t are connected to the ends of all analyzed GF chains. In these leads, a phase difference of $e^{i\theta}$ between the wavefunction amplitudes of nearest-neighbor sites is considered, where θ satisfies the dispersion relation $E=2t\cos\theta$. In Fig. 2(a)–(l), spectra of the density of states (*DOS*), zero-temperature DC conductivity [$\sigma=\sigma(\mu,0,0)$], Lyapunov coefficient (γ) and participation ratio (*PR*) are plotted as functions of the chemical potential (μ) for the three GF chains with $n=1$, null self-energies, hopping integrals of $t_A=0.8\,t$ and $t_B=t$. The lengths of these chains are given in Table 2. The used imaginary part of the energy is $\eta=10^{-5}|t|$ for *DOS* in Fig. 2(a–c), $\eta=10^{-15}|t|$ for their magnifications in Fig. 2(a′–c′), and $\eta=10^{-13}|t|$ for σ in Fig. 2(d–f). Grids of 400,000 and of 1,594,324 chemical potentials are respectively used for plotting Fig. 2(a-i) and (j-l).

Notice that all spectra of *DOS*, σ, γ, and *PR* show the same band-gap structure for each type of GF chains. In particular, the inverse of Lyapunov coefficient (γ^{-1}) of Fig. 2(g–i) reveals localization lengths very close to those of the periodic chain (γ_P^{-1}). Such behavior is confirmed by the almost ballistic DC conductivity (σ_P) in each minibands, in contrast to a general small *PR* values. In fact, they are even smaller when t_A diminishes, contrary to practically unchanged σ and γ^{-1} values in each miniband whose bandwidth decreases with t_A. Magnifications of *DOS* spectra around $\mu=0$ are further presented in Fig. 2(a′–c′) and they confirm the fractal nature of these spectra from quasiperiodic chains [9].

It is worth mentioning that the *DOS* spectrum of Fig. 2(b) for the silver mean is very close to the band structure reported in Ref. [31], in which the total band width is slightly larger than ours since their hopping integrals were $t_A=t$ and $t_B=0.8\,t$. In addition, the silver mean sequence of Ref. [31] is an isomer of ours, *i.e.*, instead of $A\to AAB$ they used a substitution rule of $A\to ABA$. In fact, the three isomers of the silver mean have almost the same *DOS* spectra. However, the localization nature of their states could be very different. For example, there are analytical solutions for the transmittance (T) at $E=0$ and they are

$$T(E=0,l)=\begin{cases}4(\chi^{p}+\chi^{-p})^{-2}, & \text{for isomer } A\to AAB\\ 4(\chi^{l}+\chi^{-l})^{-2}, & \text{for isomer } A\to ABA\\ 4(\chi^{p}+\chi^{-p})^{-2}, & \text{for isomer } A\to BAA\end{cases}, \tag{26}$$

where $\chi=t_A/t_B$, $p=[1-(-1)^l]/2$ and l is the generation number. Notice that for the case $A\to ABA$ and $\chi\neq 1$, $T(E=0,l)\to 0$ when $l\to\infty$. But for the isomers $A\to AAB$ and $A\to BAA$, $T(E=0,l)=1$ when l is an even number, regardless the value of χ. Hence, we have always transparent states at $E=0$ in these two isomers with even generation numbers.

In Figs. 3 and 4, the density of states (*DOS*), zero-temperature DC conductivity (σ), Lyapunov coefficient (γ) and participation ratio (*PR*) as functions of the chemical potential (μ) are plotted for the GF chains with $n=2$ and $n=3$, respectively. The parameters for numerical calculations are the same as in Fig. 2, except that the lengths of these chains are given in Table 2.

Notice that in Fig. 3(d–f) the DC conductivity around $\mu=0$ is almost σ_P, despite of the minimum *DOS* at the same region observed in Fig. 3(a–c). In Fig. 3(a′–c′), magnifications of *DOS* around $\mu=0$ show oscillating behaviors, in contrast to the fractal one observed in Fig. 2(a′–c′) for quasiperiodic chains.

Table 2
Number of atoms in (m,n)-type GF chains of generation l.

N	$n=1$	$n=2$	$n=3$
$m=1$	433,494,438 for $l=42$	357,913,942 for $l=29$	315,732,482 for $l=24$
$m=2$	318,281,040 for $l=23$	268,377,089 for $l=20$	581,130,734 for $l=19$
$m=3$	239,244,623 for $l=17$	253,841,390 for $l=16$	187,869,862 for $l=15$

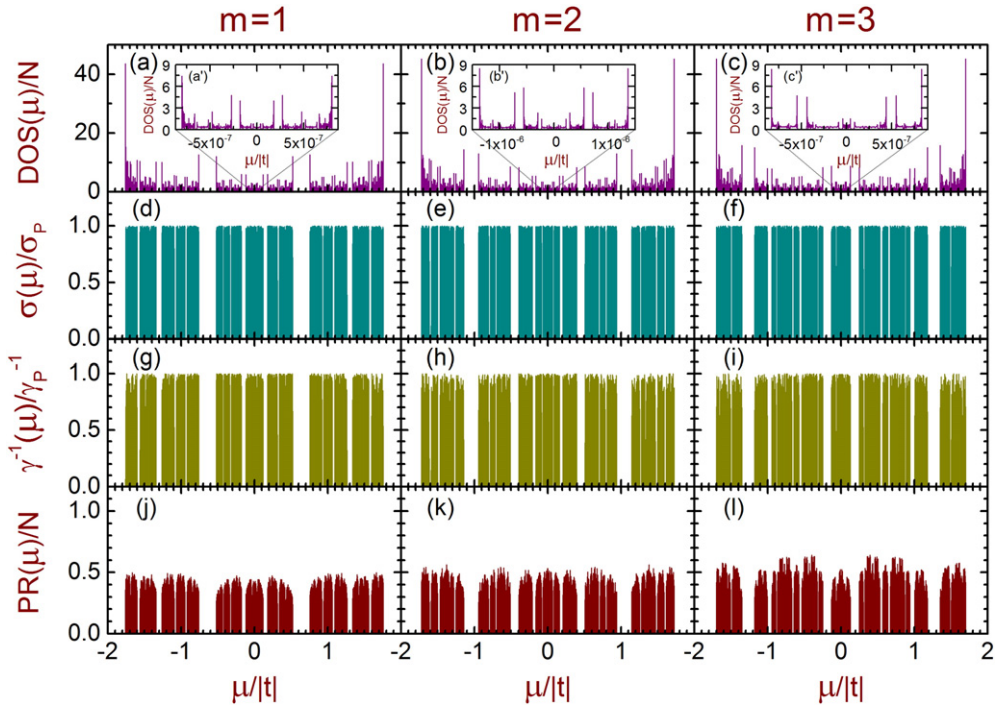

Fig. 2. Density of states (*DOS*), DC conductivity (σ), Lyapunov coefficient (γ) and participation ratio (*PR*) as functions of the chemical potential (μ) for three generalized Fibonacci chains with $n=1$, null self-energies, hopping integrals of $t_A=0.8t$ and $t_B=t$.

Contrast to Fig. 3, the high-conductivity zones in Fig. 4(d–f) are located outside the central region, correspondingly again to small values of *DOS* and an oscillating behavior as shown in Fig. 4(a′–c′). Note also that in Figs. 3 and 4, the DC conductivity (d–f), Lyapunov (g–i) and *PR* (j–l) spectra possess almost the same band structure with their high-value zones located at the same energy regions. A further analysis of *PR* for $n=2$ and $n=3$ reveals their practical constant values when the hopping integral t_A decreases, contrary to the decay behavior in *PR*

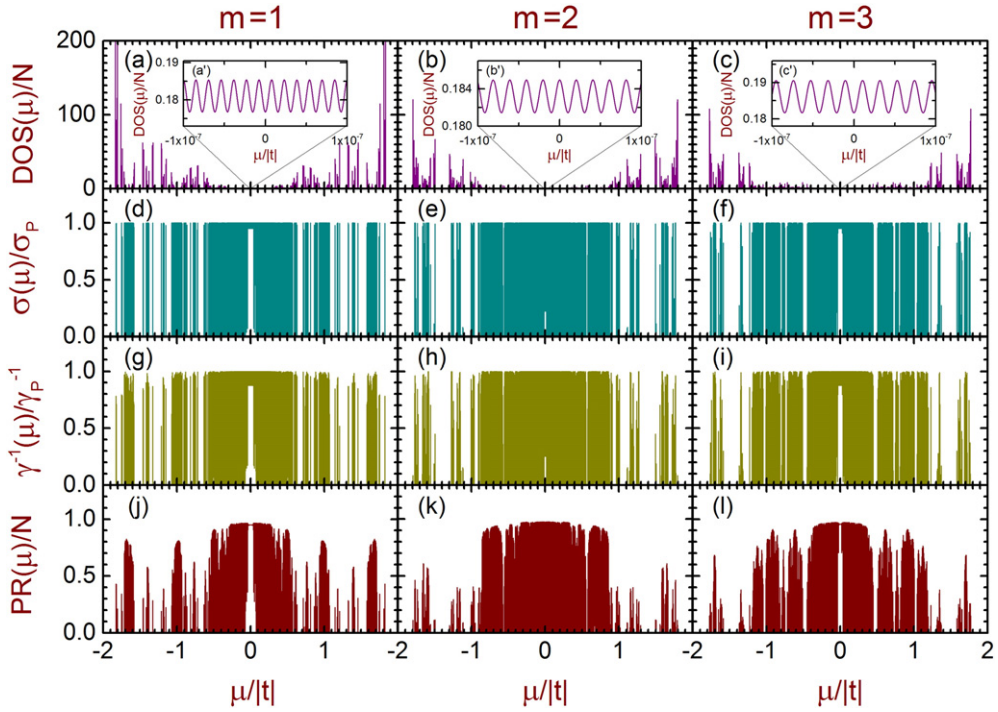

Fig. 3. Density of states (*DOS*), DC conductivity (σ), Lyapunov coefficient (γ) and participation ratio (*PR*) as functions of the chemical potential (μ) for three generalized Fibonacci chains with $n=2$, null self-energies, hopping integrals of $t_A=0.8t$ and $t_B=t$.

spectra of Fig. 2. This fact confirms the presence of almost extended states around $\mu=0$ in the (1,2) copper-mean lattice reported in reference [16].

In order to analyze the global behavior of DC conductivity (σ) and participation ratio (PR) spectra, we introduce the spectral averages of σ and of PR defined as

$$\langle\sigma\rangle = \frac{\int_{-\infty}^{\infty}\sigma(\mu)DOS(\mu)d\mu}{\int_{-\infty}^{\infty}DOS(\mu)d\mu} \quad \text{and} \quad \langle PR\rangle = \frac{\int_{-\infty}^{\infty}PR(\mu)DOS(\mu)d\mu}{\int_{-\infty}^{\infty}DOS(\mu)d\mu}. \tag{27}$$

The results of $\langle\sigma\rangle$ as functions of the system length (N) are shown in Fig. 5(a–i) for the nine GF chains of Fig. 1 with hopping integrals $t_A=t_B$ (dark yellow circles), $t_A=0.99\,t_B$ (red hexagons), $t_A=0.95\,t_B$ (blue pentagons), $t_A=0.9\,t_B$ (orange down triangles), $t_A=0.85\,t_B$ (green squares) and $t_A=0.8\,t_B$ (magenta up triangles). The imaginary part of the energy was $\eta=10^{-13}\,|t|$ for σ and $\eta=10^{-5}\,|t|$ for DOS. Observe that when the system length grows, $\langle\sigma\rangle$ is a constant for the periodic case and it decays following a power law for quasiperiodic systems with $n=1$ and it is truly archived when the system size is large enough. For other six GF systems that do not fulfill the Pisot quasiperiodic criteria, the average conductivity decay more slowly than the quasiperiodic systems, neither a constant as in periodic ones.

In Fig. 6, the spectral average of participation ratio ($\langle PR\rangle$) is plotted as functions of the number of atoms (N) in the nine GF chains of Fig. 1. The numerical calculations of $\langle PR\rangle$ were carried out by using a new renormalization method developed for the participation ratio of GF chains and presented in Appendix B. The parameters used in these calculations are the same as in Fig. 5. Observe that the $\langle PR\rangle$ results confirm the power-law and sub-power-law behaviors of $\langle\sigma\rangle$, respectively for quasiperiodic and non-quasiperiodic systems, obtained from the Kubo-Greenwood formula.

In order to perform an analytical and comparative study of PR at $\mu=0$ for (1,2)- and (2,1)-type GF chains, let us introduce the notation $PR(m,n,l)$ for a (m,n)-type GF chain of generation l evaluated at $\mu=0$, where the transfer matrices of Eq. (12) can be

$$\begin{pmatrix}0 & -\chi\\ 1 & 0\end{pmatrix},\ \begin{pmatrix}0 & -\chi^{-1}\\ 1 & 0\end{pmatrix} \text{ or } \begin{pmatrix}0 & -1\\ 1 & 0\end{pmatrix}, \tag{28}$$

with $\chi=t_A/t_B$. Hence, the normalized PR for a (2,1)-type GF chain of generation $l=2k+1$ with N_l atoms is given by

$$PR(2,1,2k+1)=\frac{\left[\sum_{j=-k}^{k-1}\Lambda_j(l)\chi^{2j}\right]^2}{N_l\sum_{j=-k}^{k-1}\Lambda_j(l)\chi^{4j}}, \tag{29}$$

where $\Lambda_j(2k+1)=2\Lambda_j(2k)+\Lambda_j(2k-1)-2\delta_{j,0}$ and $\Lambda_{-k}(l)=\frac{1}{2}[3-(-1)^l]$. At the limit of $\chi\to0$ and $l\to\infty$, we have

$$\lim_{\substack{l\to\infty\\ \chi\to0}} PR(2,1,2k+1)=\lim_{l\to\infty}\frac{\Lambda_{-k}(l)}{N_l}=0. \tag{30}$$

In contrast, the (1,2)-type GF chain has

$$PR(1,2,l)=\frac{\left[\Theta_{-1}(l)\chi^{-2}+\Theta_0(l)+\Theta_1(l)\chi^2\right]^2}{N_l\left[\Theta_{-1}(l)\chi^{-4}+\Theta_0(l)+\Theta_1(l)\chi^4\right]}, \tag{31}$$

whose coefficients Θ_{-1},Θ_0,and Θ_1 are given in Table 3.

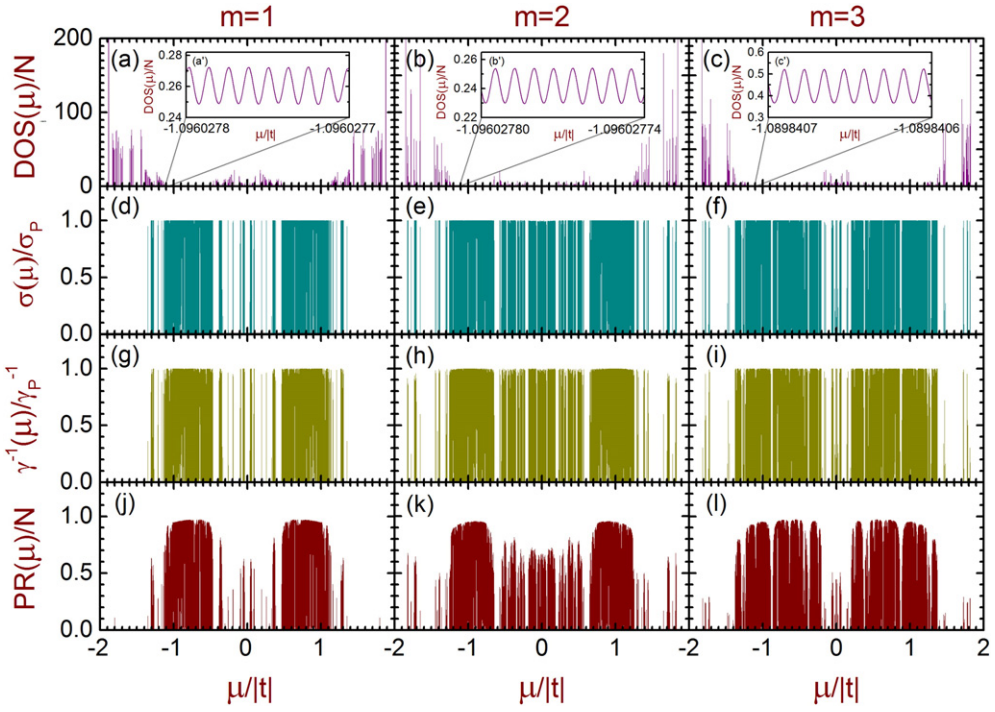

Fig. 4. Density of states (DOS), DC conductivity (σ), Lyapunov coefficient (γ) and participation ratio (PR) as functions of the chemical potential (μ) for three generalized Fibonacci chains with $n=3$, null self-energies, hopping integrals of $t_A=0.8\,t$ and $t_B=t$.

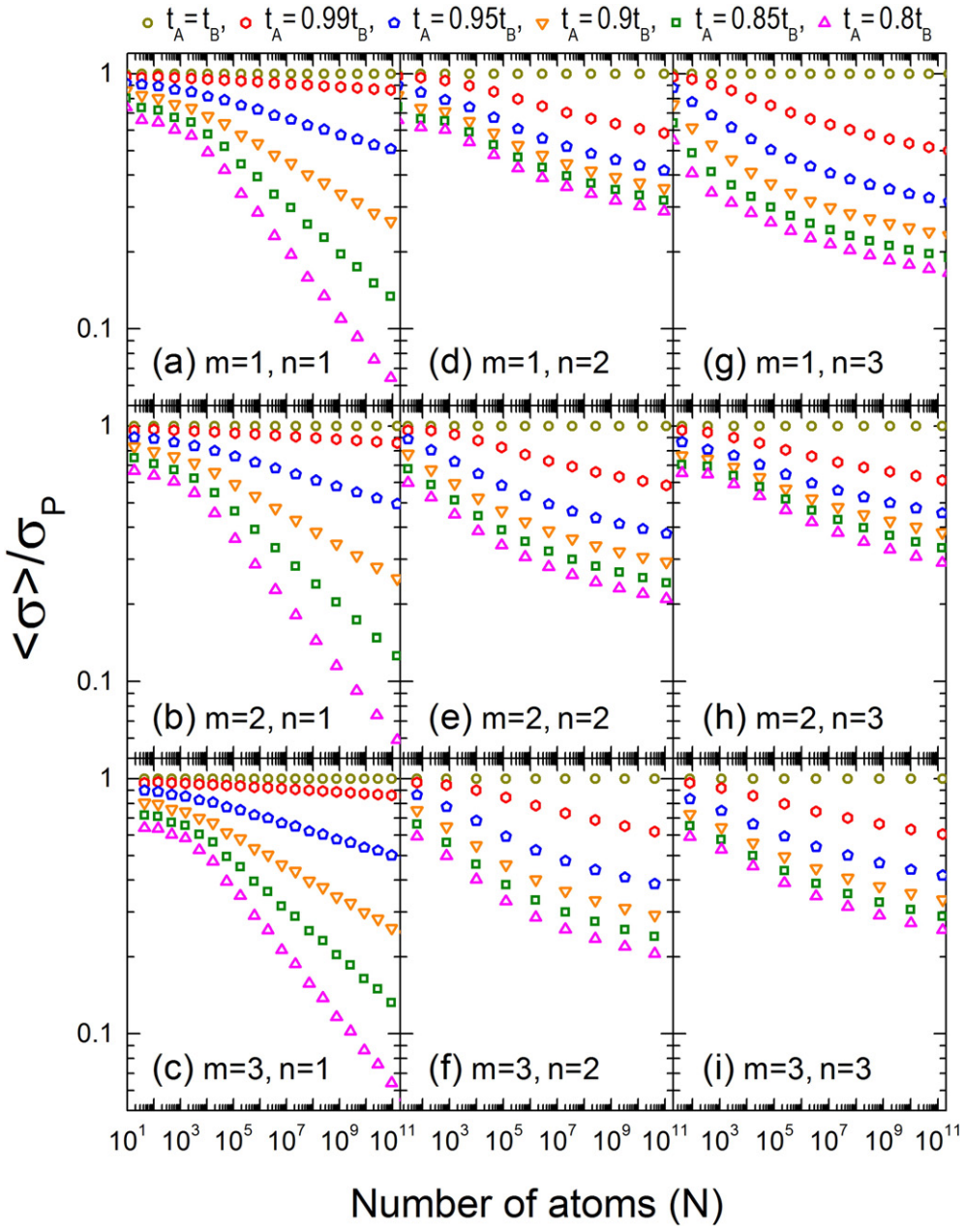

Fig. 5. Spectral average of DC conductivity ($\langle\sigma\rangle$) versus the number of atoms (N) for the nine generalized Fibonacci chains illustrated in Fig. 1 with hopping integrals $t_A = t_B$ (dark yellow solid circles), $t_A = 0.99t_B$ (red open hexagons), $t_A = 0.95t_B$ (blue open pentagons), $t_A = 0.9t_B$ (orange open down triangles), $t_A = 0.85t_B$ (green open squares) and $t_A = 0.8t_B$ (magenta open up triangles).

At the limit of $\chi \to 0$ and $l \to \infty$, Eq. (31) leads to

$$\lim_{\substack{l\to\infty \\ \chi\to 0}} PR(1,2,l) = \lim_{l\to\infty} \frac{\Theta_{-1}(l)}{N_l} = \lim_{l\to\infty} \frac{2N_{l-2} + N_{l-3} \mp 1}{N_l} = \frac{3}{8}, \tag{32}$$

because $N_l = N_{l-1} + 2N_{l-2} - 2$ and $\lim_{l\to\infty}(N_{l+1}/N_l) = 2$. The analytical results of Eqs. (30) and (32) confirm the numerical ones shown in Figs. 2 and 3.

5. AC conductivity

As observed in Figs. 2, 3 and 4, there are many peaks in DC conductivity (σ) spectra. If we choose a chemical potential (μ) located between two successive peaks and an external alternating electrical field with $\hbar\omega$ equal to the difference between their energies, a resonant AC electronic transport is registered in segmented [32] and branched nanowires [19]. In this section, we analyze such transport in GF chains. Fig. 7 shows AC conductivity spectra in color scale versus the chemical potential (μ) and the electrical field frequency (ω) for GF chains with $t_A = 0.8t$, $t_B = t$ (a) $m = 1$, $n = 1$ and $l = 14$; (b) $m = 2$, $n = 2$ and $l = 7$; (c) $m = 3$, $n = 3$ and $l = 5$. The calculations were performed by using an imaginary part of energy $\eta = 10^{-15}|t|$ and these GF chains are connected to two semi-infinite periodic leads with hopping integrals of t.

Observe in Fig. 7(a) a band structure at low frequency limit similar to that of Fig. 2(d). For several frequencies, red zones with an AC conductivity larger than the ballistic one $\sigma_P(\mu,\omega,0)$ of periodic chain given by Eq. (20) can be found. For example, in Fig. 7(a) there is a resonant peak of $\sigma(\mu,\omega,0) = 1.755\,\sigma_P$ (red bar) at $\hbar\omega = 0.06123246|t|$ for

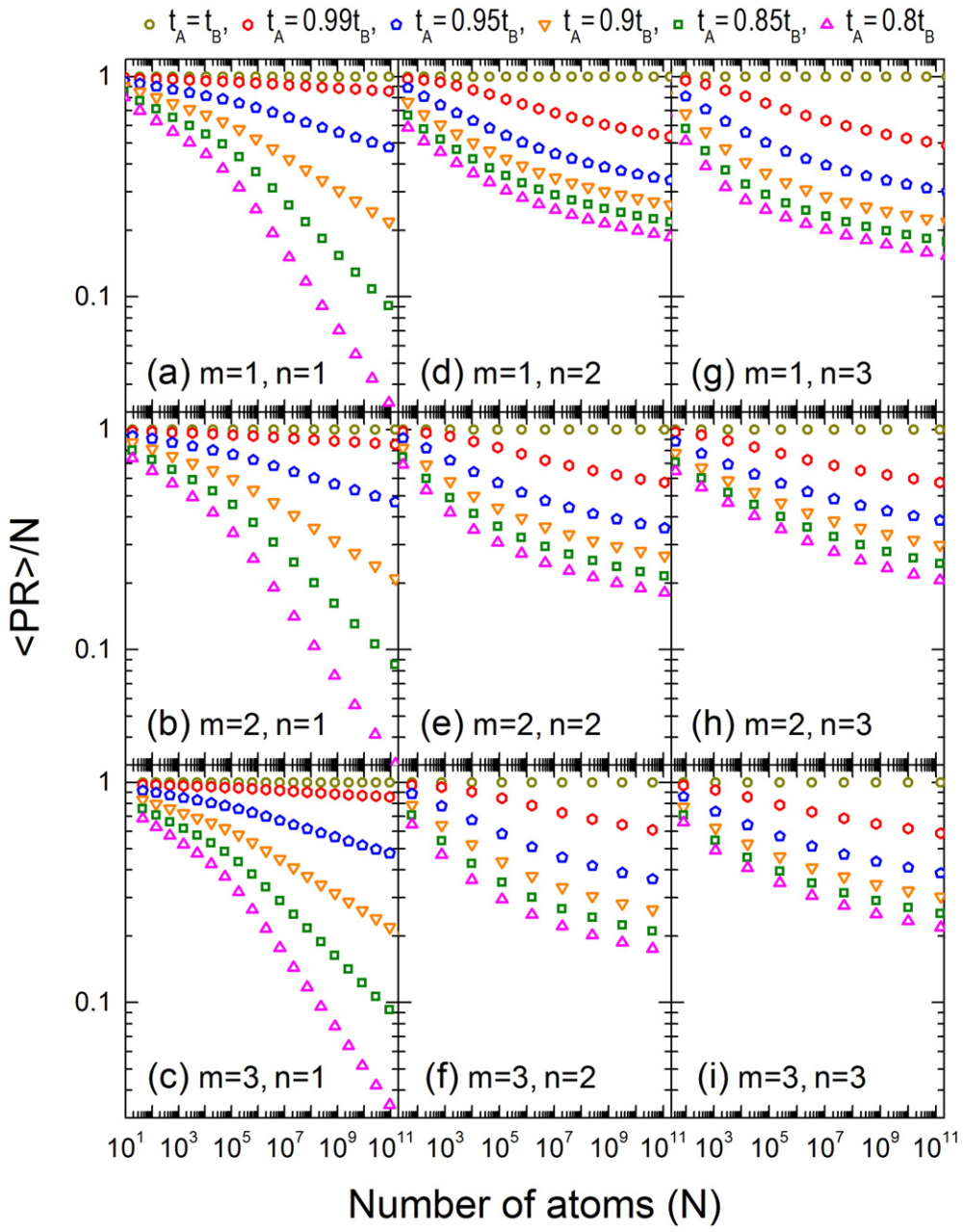

Fig. 6. Spectral average of participation ratio ($\langle PR \rangle$) versus the number of atoms (N) for the nine generalized Fibonacci chains illustrated in Fig. 1 with hopping integrals $t_A = t_B$ (dark yellow solid circles), $t_A = 0.99t_B$ (red open hexagons), $t_A = 0.95t_B$ (blue open pentagons), $t_A = 0.9t_B$ (orange open down triangles), $t_A = 0.85t_B$ (green open squares) and $t_A = 0.8t_B$ (magenta open up triangles).

$0.11738557|t| \le \mu \le 0.17861803|t|$, whose conductivity quickly decays with the diminution or the increase of frequency. Close to this red bar, there is another resonant peak of $\sigma(\mu, \omega, 0) = 0.384\sigma_P$ (green bar) at $\hbar\omega = 0.06745621|t|$ for $0.11400161|t| \le \mu \le 0.18145782|t|$. The first one is originated by an interband excitation between two high DC conduction states at $E = 0.11738557|t|$ and $E = 0.17861803|t|$ just located at the borders of a bandgap, while the second one is due to third neighbor peaks of high DC conductions located at $E = 0.11400161|t|$ and $E = 0.18145782|t|$. In fact, there are resonant AC conductions when $\hbar\omega$ is equal to the energy difference corresponding to DC conductivity peaks separated by an even number of peaks in the DC conductivity spectrum, as shown in Fig. 3 of Ref. [19]. Furthermore, notice in Fig. 7(b) and (c) the presence of color zones with AC conductivity $0.2\sigma_P \le \sigma(\mu, \omega, 0) \le 0.9\sigma_P$, caused by resonances between rounded peaks shown in Figs. 3(b′) and 4(c′) separated by an energy of the order of $|t|/N$, in contrast to sharp peaks in Fig. 2(a′) leading to well defined resonant frequencies in Fig. 7(a). In general, high resonant AC conductivities have been found at the extremes of bands.

Table 3
Coefficients Θ_i of term χ^i in Eq. (31) for (1,2)-type GF chains.

$m=1, n=2$	l even	l odd
$\Theta_{-1}(l)$	$2N_{l-2} - N_{l-3} - 1$	$2N_{l-2} - N_{l-3} + 1$
$\Theta_0(l)$	$N_{l-1} - 1$	$N_{l-1} - 2$
$\Theta_1(l)$	N_{l-3}	$N_{l-3} - 1$

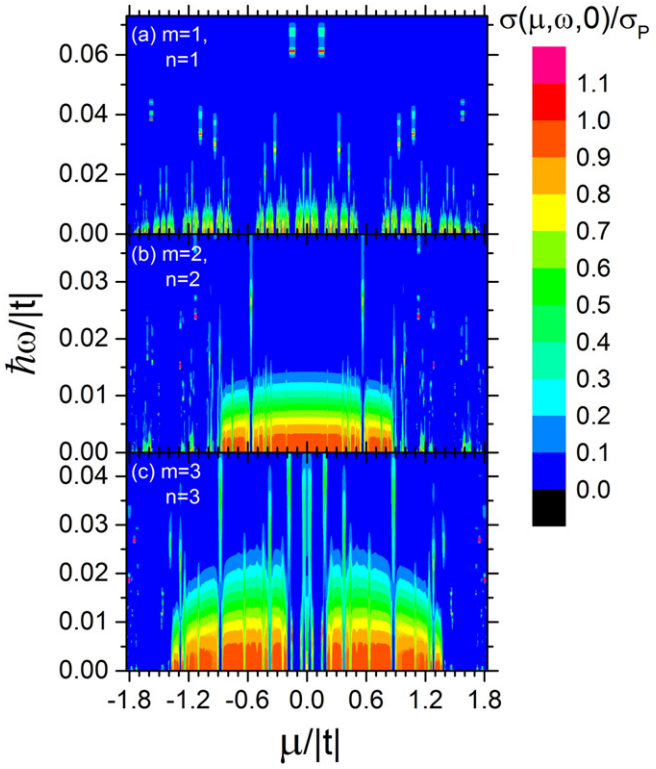

Fig. 7. AC conductivity spectra (in color scale) versus chemical potential (μ) and frequency (ω) for generalized Fibonacci chains with (a) $m=1, n=1$ and $l=14$, (b) $m=2, n=2$ and $l=7$, (c) $m=3, n=3$ and $l=5$.

In order to compare the global resonant AC conduction capability in different GF chains, we introduce a spectral average conductivity defined as

$$<\sigma(\mu,\omega,0)> = \frac{1}{N_{pk}-1}\sum_{j=1}^{N_{pk}-1}\sigma(\mu_j,\omega_j,0), \tag{33}$$

where N_{pk} is the total number of peaks in the DC conductivity spectrum, $\mu_j=(E_{j+1}+E_j)/2$ and $\omega_j=(E_{j+1}-E_j)/\hbar$ are respectively the central energy and the resonant frequency of two successive DC conductivity peaks with energies of E_j and E_{j+1}. Fig. 8 show $<\sigma(\mu,\omega,0)>$ (open circles) versus the number of atoms (N) in nine GF chains, where the error bars illustrate the maximum and minimum values of AC conductivities in each generation (l). Observe that $\langle\sigma(\mu,\omega,0)\rangle$ grows with the number of atoms and the maximum AC conductivity can reach to 10^{10} times the ballistic DC conductivity (σ_P) for non-quasiperiodic GF chains of 10^5 atoms. In fact, the zero-temperature ballistic AC conductivity $\sigma_P(\mu,\omega,0)$ of periodic chains is bounded by σ_P. Overall, the truly high AC conductivities were obtained from the resonance of very sharp DC conductivity peaks.

6. Generalized Fibonacci nanowires

The electronic transport in aperiodic nanowires with finite cross-section can be studied by using the renormalization plus convolution method for the Kubo-Greenwood formula and its electrical conductivity (σ) is expressed as [30]

$$\sigma(\mu,\omega,T) = \frac{1}{\Omega_\perp}\sum_\beta \sigma^{\parallel}(\mu-E_\beta,\omega,T), \tag{34}$$

where $\sigma^{\parallel}$ is the electrical conductivity of the parallel subsystem, $\Omega_\perp$ and E_β are respectively the volume and the eigenenergies of the

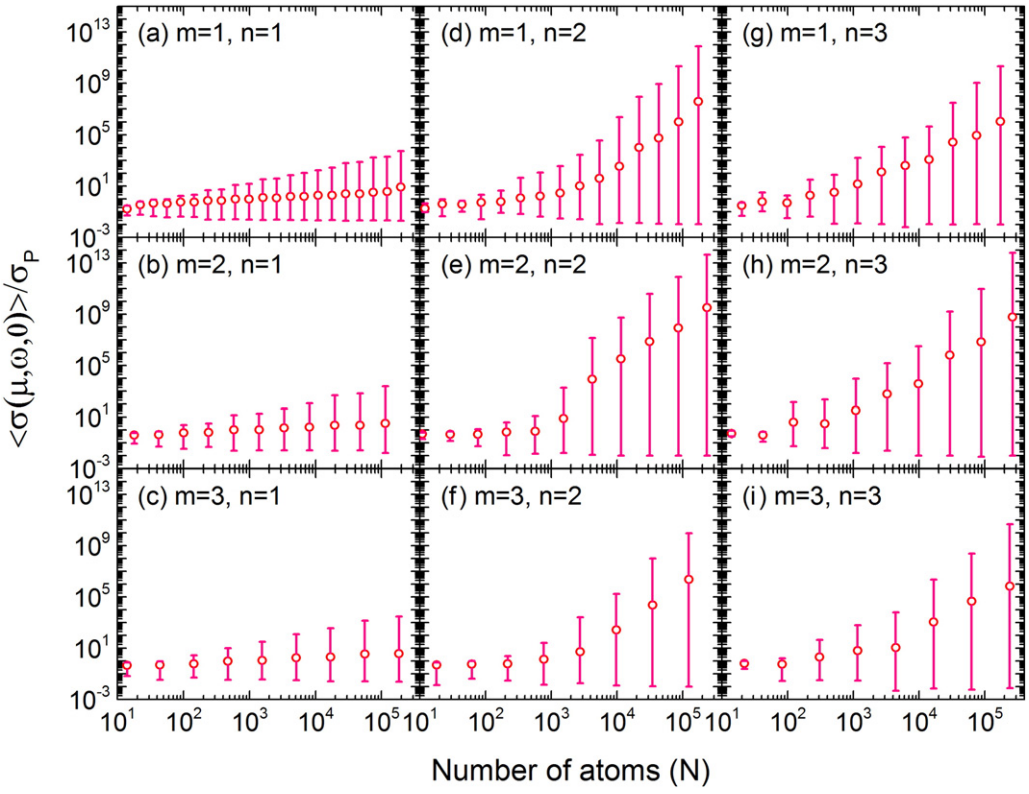

Fig. 8. Spectral averages of zero-temperature AC conductivity $\langle\sigma(\mu,\omega,0)\rangle$ (open circles) versus the number of atoms (N) for nine generalized Fibonacci chains of type (m,n), where the error bars indicate the maximum and minimum AC conductivity values.

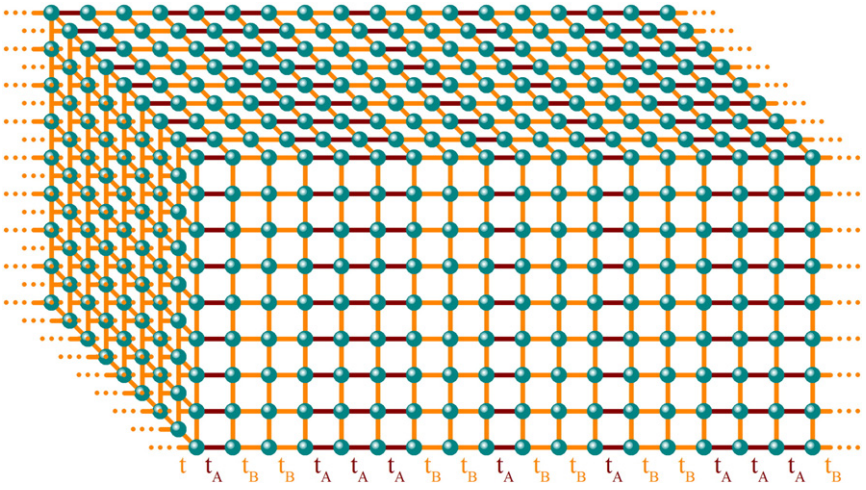

Fig. 9. Sketch of a segment of a nanowire with a periodic cross section of 9×9 atoms, whose hopping integrals t_A and t_B along the longitudinal direction follow the copper-mean sequence.

perpendicular subsystem. The electrical conductance is written as $g(\mu,\omega,T)\equiv\sigma(\mu,\omega,T)\Omega_\perp/\Omega_\parallel$, where $\Omega_\parallel$ is the length of the nanowire. For example, a nanowire with a periodic cross section of 9×9 atoms is shown in Fig. 9, whose hopping integrals t_A and t_B along the longitudinal direction of nanowire are ordered following the copper-mean sequence with $m=1$ and $n=2$.

The zero-temperature DC conductance (g) as a function of the chemical potential (μ) is presented in Fig. 10 for nine GF nanowires with cross sections of 9 × 9 atoms (see Fig. 9), whose longitudinal arrangements of hopping integrals follow the sequences shown in Fig. 1. The lengths of these nanowires are specified in Table 2 and the Hamiltonian parameters are $t_A=0.8\,t$, $t_B=t$ and null self-energies. The imaginary part of the energy is $\eta=10^{-15}|t|$ and Fig. 10 are plotted by using a grid of 120,000 chemical potentials. The conductance g spectra, normalized by the quantum of conductance $g_0\equiv 2e^2/h$, of GF nanowires are compared to that of a periodic nanowire with the same cross section (light grey lines). Observe its quantized conductance, in which the step height in unity of g_0 at $\pm(|E_\beta|+2|t|)$ is the degeneracy of E_β. In particular, the maximum step height is $9g_0$ located at $\mu=\pm 2|t|$, since the cross section is of 9 × 9 atoms. Moreover, the integral $\int_{-\infty}^{\infty} g(\mu,0,0)d\mu$ of this stepped spectrum is $324g_0|t|$, because each of the 81 ballistic conducting channels provides a constant area of $4g_0|t|$ wherever it is placed. When the arrangement of hopping integrals follows a quasiperiodic sequence along the longitudinal direction, the conductance is significantly smaller than the periodic case. In general, the non-quasiperiodic nanowires with $n>1$ have larger electrical conductance

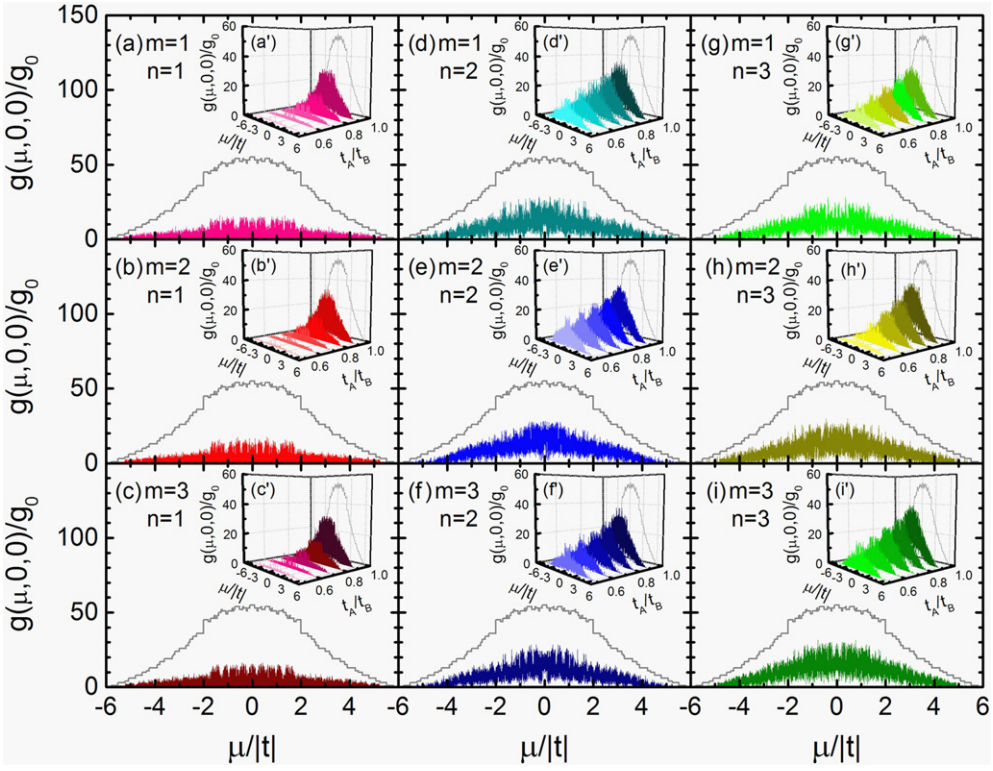

Fig. 10. Zero-temperature electrical conductance (g) versus the chemical potential (μ) for nine GF nanowires of type (m,n) with cross sections of 9×9 atoms, $t_A=0.8\,t$, $t_B=t$, null self-energies, whose longitudinal arrangements of hopping integrals follow the sequences of Fig. 1. These spectra are compared to that of a periodic nanowire with the same cross section (light gray lines). Insets: Corresponding conductance spectra for $t_A/t_B=0.5$, 0.6, 0.7, 0.8, 0.9 and 1.0.

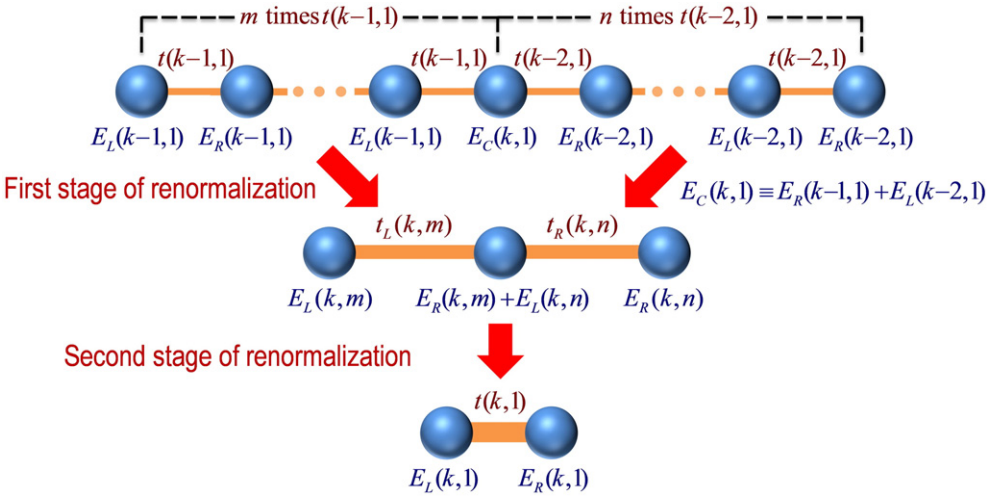

Fig. A1. Schematic representation of the two-stage renormalization procedure for generalized Fibonacci chains of type (m,n).

than those of quasiperiodic ones with $n=1$, in consistence with the single-channel spectral-average results of Fig. 5. In fact, they have large intervals of μ with $g(\mu,0,0)>0$, in contrast to the almost zero minimum value of g over whole spectra for quasiperiodic nanowires, which could be related to the eigenvalue spectra supported on Cantor sets of Lebesgue measure zero for quasiperiodic chains with site disorder [33]. Finally, the insets of Fig. 10 show the evolution of electrical conductance spectra when the bond disorder amplitude of GF nanowires grows. Observe the rapid vanish of conductance spectra of quasiperiodic nanowires in comparison to the non-quasiperiodic ones.

7. Conclusions

To quantify the localization of wavefunctions in macroscopic generalized Fibonacci (GF) systems, we have developed a new real-space renormalization method for the participation ratio (*PR*). Also, we have extended the renormalization method previously developed for the Kubo-Greenwood formula in Fibonacci lattices [30] with $n=m=1$ to all (m,n)-type GF ones. In general, these renormalization methods have the advantage of being computationally efficient without introducing additional approximations and representing a useful alternative for the study of non-periodic systems, where the reciprocal space is absent or useless.

The *PR* has been one of the most used quantities for the study of wavefunction localization in disordered systems and the results of this article reveal its deficiency in quasiperiodic lattices. In particular, we found a transparent state at $\mu=0$ in (2,1)-type GF chains for any even number of generation [34] and $\chi=t_A/t_B>0$. However, the corresponding *PR* has a limiting value of zero, as demonstrated in Eq. (30). In other words, an extremely localized electronic state with almost zero *PR* could possess a ballistic transport. In general, the results confirm the close relation, with the possible exception of critically localized states [9], between the wavefunction localization and the electronic transport at zero temperature. For example, the close resemblance between DC conductivity spectra and Lyapunov exponent ones. In particular, they are self-similar for the GF chains with $n=1$, in accordance to their purely singular continuous spectra established for the site problem [33]. This fact leads to a power-law decay of the spectral averages of both DC conductivity and *PR* when the number of atoms increases. In contrast, GF chains with $n=2$ and $n=3$ present zones with high-conduction oscillating behavior, which gives rise a slow decay of these spectral averages. In addition, we found an analytical expression of Lyapunov exponent for periodic lattices.

Finally, we report the first global analysis of AC conduction over entire spectra of GF chains. The results show extremely high resonant AC conductivity peaks in comparison to the ballistic AC one, whose average value grows faster in non-quasiperiodic systems than quasiperiodic ones. In general, partially localized electronic states could favor the interaction with external oscillating electric fields through local electric dipoles, inducing a larger AC response than a homogeneous charge distribution in periodic systems. Hence, the spatial localization of states determines their resonance intensity via the Fermi's golden rule, from which the Kubo-Greenwood formula can be obtained [26]. This study of the correlation between wavefunction localization and electronic transport can be extended to multidimensional systems, as partially done in Section VI for the DC conductivity of GF nanowires by using the convolution theorem.

Table A1
Significance of symbols in Eq. (A.2).

Stage	α	β	ε	δ	λ	ξ	ζ
First	L	L	F	$j-1$	j	$k-1$	1
	R	R				$k-2$	
Second	F	L	R	m	1	k	n

Acknowledgements

We would like to acknowledge Dr. Carlos Ramirez for the useful discussions. This work has been partially supported by CONACyT-252943 and by UNAM-DGAPA-PAPIIT through IN113714 and IN114916. Computations were performed at Miztli of DGTIC-UNAM.

Appendix A. Renormalization formulas for the density of states

For a generalized Fibonacci (GF) chain of type (m,n) with two kinds of bonds, t_A and t_B, the density of states (*DOS*) of generation l evaluated at energy E in terms of the Green's function (G) can be written as in Ref. [30],

$$\begin{aligned} DOS(E,l) &= -\frac{1}{\pi}\lim_{\eta\to 0^+}\mathrm{Im}\sum_{j=1}^{N(l)}G_{j,j}(z) \\ &= -\frac{1}{\pi}\lim_{\eta\to 0^+}\mathrm{Im}[A_F(l,1)G_{L,L}(z)+B_F(l,1)G_{R,R}(z) \\ &\quad +C_F(l,1)G_{L,R}(z)+D_F(l,1)] \end{aligned} \tag{A.1}$$

where $z=E+i\eta$, $N(l)$ is the total number of atoms in a GF chain of generation l, and the coefficients A, B, C and D are iteratively calculated by

means of a two-stage renormalization procedure, as schematically summarized in Fig. A1, through

$$\begin{cases} A_\alpha(k,\lambda) = A_\beta(k,\delta) + \theta_\alpha^2(k,\lambda)[A_\varepsilon(\xi,\zeta) \\ \quad +B_\beta(k,\delta)-1] + \theta_\alpha(k,\lambda)C_\beta(k,\delta) \\ B_\alpha(k,\lambda) = B_\varepsilon(\xi,\zeta) + \phi_\alpha^2(k,\lambda)[A_\varepsilon(\xi,\zeta) \\ \quad +B_\beta(k,\delta)-1] + \phi_\alpha(k,\lambda)C_\varepsilon(\xi,\zeta) \\ C_\alpha(k,\lambda) = \phi_\alpha(k,\lambda)C_\beta(k,\delta) + \theta_\alpha(k,\lambda)C_\varepsilon(\xi,\zeta) \\ \quad +2\theta_\alpha(k,\lambda)\phi_\alpha(k,\lambda)\left[A_\varepsilon(\xi,\zeta) + B_\beta(k,\delta)-1\right] \\ D_\alpha(k,\lambda) = D_\beta(k,\delta) + D_\varepsilon(\xi,\zeta) + [A_\varepsilon(\xi,\zeta) \\ \quad +B_\beta(k,\delta)-1]/[z-E_R(k,\delta)-E_L(\xi,\zeta)] \end{cases}, \tag{A.2}$$

where

$$\begin{cases} \theta_\alpha(k,\lambda) = t_\beta(k,\delta)/[z-E_R(k,\delta)-E_L(\xi,\zeta)] \\ \phi_\alpha(k,\lambda) = t_\varepsilon(\xi,\zeta)/[z-E_R(k,\delta)-E_L(\xi,\zeta)] \\ E_L(k,\lambda) = E_L(k,\delta) + t_\beta^2(k,\delta)/[z-E_R(k,\delta) \\ \quad -E_L(\xi,\zeta)] \\ E_R(k,\lambda) = E_\varepsilon(\xi,\zeta) + t_\varepsilon^2(\xi,\zeta)/[z-E_R(k,\delta) \\ \quad -E_L(\xi,\zeta)] \\ t_\alpha(k,\lambda) = t_\beta(k,\delta)t_\varepsilon(\xi,\zeta)/[z-E_R(k,\delta) \\ \quad -E_L(\xi,\zeta)] \end{cases} \tag{A.3}$$

and the significance of $\alpha,\beta,\varepsilon,\delta,\lambda,\xi$ and ζ are given in Table A1, where in each row the value of α determines the meaning of the subsequent parameters.

For a GF chain of generation k, the renormalization procedure consists of using the same Eqs. (A.2)–(A.3) and following the steps: (1) iteratively calculating the coefficients $A_L(k-1,j)$, $B_L(k-1,j)$, $C_L(k-1,j)$ and $D_L(k-1,j)$ for $j=2,\ 3,\cdots,\ m$; (2) iteratively computing $A_R(k-2,j)$, $B_R(k-2,j)$, $C_R(k-2,j)$ and $D_R(k-2,j)$ for $j=2,\ 3,\cdots,\ n$; and (3) using the results of left- and right-segment renormalizations to calculate $A_F(k,1)$, $B_F(k,1)$, $C_F(k,1)$ and $D_F(k,1)$ of generation k. This calculation should be repeated for $k=2,\ 3,\ \cdots,\ l$ in order to finally determine the *DOS* of a GF chain of type (m,n) and generation l.

The initial conditions for Eqs. (A.2)–(A.3) are $t_F(0,1)=t_B$, $A_F(0,1)=B_F(0,1)=1$, $C_F(0,1)=D_F(0,1)=0$, $E_L(0,1)=E_R(0,1)=0$, $A_F(1,1)=B_F(1,1)=1$, $C_F(1,1)=D_F(1,1)=0$, $t_F(1,1)=t_A$, and $E_L(1,1)=E_R(1,1)=0$.

When the system is connected to two periodic leads, the Green's functions at its extreme atoms are given by

$$G_{L,L}(z) = \left\{ z-E_L(l,1)-E_P^R(l')-\frac{t_P^2(l')}{z-E_P^L(l')} - \frac{t_F^2(l,1)}{z-E_R(l,1)-E_P^L(l')-t_P^2(l')/\left[z-E_P^R(l')\right]} \right\}^{-1}, \tag{A.4}$$

$$G_{R,R}(z) = \left\{ z-E_R(l,1)-E_P^L(l')-\frac{t_P^2(l')}{z-E_P^R(l')} - \frac{t_F^2(l,1)}{z-E_L(l,1)-E_P^R(l')-t_P^2(l')/\left[z-E_P^L(l')\right]} \right\}^{-1}, \tag{A.5}$$

and

$$G_{L,R}(z) = \frac{t_F(l,1)G_{R,R}(z)}{z-E_L(l,1)-E_P^R(l')-t_P^2(l')/\left[z-E_P^L(l')\right]}, \tag{A.6}$$

where l' is the generation number of these periodic leads built following the GF renormalization procedure with $m=n=1$ and $t_A=t_B=t$, whose effective self-energies and hopping-integrals are $E_P^L(l')=E_P^L(l'-1)+t_P^2(l'-1)\gamma_P$, $E_P^R(l')=E_P^R(l'-2)+t_P^2(l'-2)\gamma_P$, and $t_P(l')=t_P(l'-1)\,t_P(l'-2)\gamma_P$, being $\gamma_P=[z-E_P^R(l'-1)-E_P^L(l'-2)]^{-1}$.

In order to illustrate the procedure for obtaining the renormalization formulas, we may take the middle state of Fig. A1 as the initial system, whose *DOS* can be written from Eq. (A.1) as

$$DOS(E,l) = -\frac{1}{\pi}\lim_{\eta\to 0^+}\mathrm{Im}\begin{bmatrix} \sum_{j=1}^{mN(l-1)}G_{j,j}(z) \\ +\sum_{j=mN(l-1)}^{N(l)}G_{j,j}(z) \\ -G_{C,C}(z) \end{bmatrix} \tag{A.7}$$

$$= -\frac{1}{\pi}\lim_{\eta\to 0^+}\mathrm{Im}\begin{bmatrix} A_L(l,m)G_{L,L}(z) + B_L(l,m)G_{C,C}(z) \\ +C_L(l,m)G_{L,C}(z) + D_L(l,m)+ \\ A_R(l,n)G_{C,C}(z) + B_R(l,n)G_{R,R}(z) \\ +C_R(l,n)G_{C,R}(z) \\ +D_R(l,n)-G_{C,C}(z) \end{bmatrix},$$

where the Green's function elements satisfy the Dyson's equation given by

$$\begin{pmatrix} z-E_L(l,m) & -t_L(l,m) & 0 \\ -t_L(l,m) & z-E_C(l,1) & -t_R(l,n) \\ 0 & -t_R(l,n) & z-E_R(l,n) \end{pmatrix}\times \begin{pmatrix} G_{L,L}(z) & G_{L,C}(z) & G_{L,R}(z) \\ G_{C,L}(z) & G_{C,C}(z) & G_{C,R}(z) \\ G_{R,L}(z) & G_{R,C}(z) & G_{R,R}(z) \end{pmatrix} = \begin{pmatrix} 1 & 0 & 0 \\ 0 & 1 & 0 \\ 0 & 0 & 1 \end{pmatrix}. \tag{A.8}$$

In other words,

$$G_{C,X}(z) = \frac{\delta_{C,X}}{z-E_C(l,1)} + \frac{t_L(l,m)}{z-E_C(l,1)}G_{L,X}(z) + \frac{t_R(l,n)}{z-E_C(l,1)}G_{R,X}(z), \tag{A.9}$$

where $X=L,C$, or R, and $E_C(l,1)=E_R(l,m)+E_L(l,n)$. Taking the advantage of being the Green's function a symmetric matrix derived from a symmetric Hamiltonian, Eq. (A.9) for $X=C$ can be rewritten by using the same equation for $X=L$ and $X=R$ as

$$G_{C,C}(z) = [z-E_C(l,1)]^{-1} + \theta_F^2(l,1)G_{L,L}(z) + \phi_F^2(l,1)G_{R,R}(z) + 2\theta_F(l,1)\phi_F(l,1)G_{L,R}(z). \tag{A.10}$$

Substituting Eqs. (A.9)–(A.10) into Eq.(A.7), one obtains

$$\begin{aligned} DOS(E,l) = -\frac{1}{\pi}\lim_{\eta\to 0^+}\mathrm{Im}\{&A_L(l,m)G_{L,L}(z) \\ &+D_L(l,m) + D_R(l,n) + B_R(l,n)G_{R,R}(z) \\ &+C_L(l,m)\left[\theta_F(l,1)G_{L,L}(z) + \phi_F(l,1)G_{R,L}(z)\right] \\ &+C_R(l,n)\left[\theta_F(l,1)G_{L,R}(z) + \phi_F(l,1)G_{R,R}(z)\right] \\ &+[B_L(l,m) + A_R(l,n)-1][\theta_F^2(l,1)G_{L,L}(z) \\ &+\phi_F^2(l,1)G_{R,R}(z) + 2\theta_F(l,1)\phi_F(l,1)G_{L,R}(z) \\ &+[z-E_C(l,1)]^{-1}]\}, \end{aligned} \tag{A.11}$$

which leads to Eq. (A.2). On the other hand, substituting Eqs. (A.9) into Eq. (A.8), it becomes to

$$\begin{pmatrix} z-E_L(l,1) & -t_F(l,1) \\ -t_F(l,1) & z-E_R(l,1) \end{pmatrix}\times \begin{pmatrix} G_{L,L}(z) & G_{L,R}(z) \\ G_{R,L}(z) & G_{R,R}(z) \end{pmatrix} = \begin{pmatrix} 1 & 0 \\ 0 & 1 \end{pmatrix}, \tag{A.12}$$

where the renormalized hopping integral $t_F(l,1)$ and self-energies, $E_L(l,1)$ and $E_R(l,1)$, are given in Eq. (A.3).

Appendix B. Renormalization formulas for the participation ratio

Since the single-electron wavefunction ($|\Psi\rangle$) can be written as a linear combination of the Wannier's function ($|j\rangle$) of atom j, $|\Psi\rangle = \sum_j c_j|j\rangle$, the participation ratio (PR) for a non-normalized wavefunction is given by

$$PR = \frac{\left(\sum_j |c_j|^2\right)^2}{\sum_j |c_j|^4} \tag{B.1}$$

and its denominator may be expressed in term of the wavefunction amplitudes at extreme sites, c_L and c_R, as

$$\begin{aligned}\textstyle\sum_j |c_j|^4 = {} & I_F(l,1)|c_L|^4 + L_F(l,1)\left[c_L^2 c_R^{*2} + c_R^2 c_L^{*2}\right] \\ & + J_F(l,1)|c_R|^4 + P_F(l,1)|c_L|^2\left(c_L c_R^* + c_R c_L^*\right) + \\ & K_F(l,1)|c_L|^2|c_R|^2 + Q_F(l,1)|c_R|^2\left(c_L c_R^* + c_R c_L^*\right),\end{aligned} \tag{B.2}$$

where $I_F(l,1)$, $J_F(l,1)$, $K_F(l,1)$, $L_F(l,1)$, $P_F(l,1)$ and $Q_F(l,1)$ are the renormalization coefficients for PR. Analogously, the normalization condition of wavefunction $|\Psi\rangle$ can also be expressed as

$$\begin{aligned}1 = \sum_j |c_j|^2 = {} & R_F(l,1)|c_L|^2 + S_F(l,1)|c_R|^2 \\ & + U_F(l,1)[c_L c_R^* + c_R c_L^*].\end{aligned} \tag{B.3}$$

Following a similar renormalization procedure for the DOS explained at the end of Appendix A, by using the Schrödinger equation instead of the Dyson one, the renormalization coefficients for PR of a (m,n)-type GF chain of generation l can be iteratively calculated for $k = 2, 3, \cdots, l$ by means of

$$\begin{aligned}I_\alpha(k,\lambda) = {} & \theta_\alpha^3(k,\lambda)\Big\{\theta_\alpha(k,\lambda)\Big[J_\beta(k,\delta) + I_\varepsilon(\xi,\zeta) - 1\Big] \\ & + 2Q_\beta(k,\delta)\Big\} + I_\beta(k,\delta) + 2\theta_\alpha(k,\lambda)P_\beta(k,\delta) \\ & + \theta_\alpha^2(k,\lambda)\left[K_\beta(k,\delta) + 2L_\beta(k,\delta)\right],\end{aligned} \tag{B.4}$$

$$\begin{aligned}J_\alpha(k,\lambda) = {} & \phi_\alpha^3(k,\lambda)\Big\{\phi_\alpha(k,\lambda)\Big[J_\beta(k,\delta) + I_\varepsilon(\xi,\zeta) - 1\Big] \\ & + 2P_\varepsilon(\xi,\zeta)\Big\} + J_\varepsilon(\xi,\zeta) + 2\phi_\alpha(k,\lambda)Q_\varepsilon(\xi,\zeta) \\ & + \phi_\alpha^2(k,\lambda)[K_\varepsilon(\xi,\zeta) + 2L_\varepsilon(\xi,\zeta)],\end{aligned} \tag{B.5}$$

$$\begin{aligned}K_\alpha(k,\lambda) = {} & \theta_\alpha^2(k,\lambda)\Big\{4\phi_\alpha^2(k,\lambda)\Big[J_\beta(k,\delta) + I_\varepsilon(\xi,\zeta) - 1\Big] \\ & + K_\varepsilon(\xi,\zeta) + 4\phi_\alpha(k,\lambda)P_\varepsilon(\xi,\zeta)\Big\} \\ & + \phi_\alpha^2(k,\lambda)\left[K_\beta(k,\delta) + 4\theta_\alpha(k,\lambda)Q_\beta(k,\delta)\right],\end{aligned} \tag{B.6}$$

$$\begin{aligned}L_\alpha(k,\lambda) = {} & \theta_\alpha^2(k,\lambda)\Big\{\phi_\alpha^2(k,\lambda)\Big[J_\beta(k,\delta) + I_\varepsilon(\xi,\zeta) - 1\Big] \\ & + L_\varepsilon(\xi,\zeta) + \phi_\alpha(k,\lambda)P_\varepsilon(\xi,\zeta)\Big\} \\ & + \phi_\alpha^2(k,\lambda)\left[L_\beta(k,\delta) + \theta_\alpha(k,\lambda)Q_\beta(k,\delta)\right],\end{aligned} \tag{B.7}$$

$$\begin{aligned}P_\alpha(k,\lambda) = {} & \theta_\alpha^3(k,\lambda)\Big\{2\phi_\alpha(k,\lambda)\Big[J_\beta(k,\delta) + I_\varepsilon(\xi,\zeta) - 1\Big] \\ & + P_\varepsilon(\xi,\zeta)\Big\} + \theta_\alpha(k,\lambda)\phi_\alpha(k,\lambda)\{[K_\beta(k,\delta) + \\ & 2L_\beta(k,\delta)] + 3\theta_\alpha(k,\lambda)Q_\beta(k,\delta)\Big\} + \phi_\alpha(k,\lambda)P_\beta(k,\delta),\end{aligned} \tag{B.8}$$

$$\begin{aligned}Q_\alpha(k,\lambda) = {} & \phi_\alpha^3(k,\lambda)\Big\{2\theta_\alpha(k,\lambda)\Big[J_\beta(k,\delta) + I_\varepsilon(\xi,\zeta) - 1\Big] \\ & + Q_\beta(k,\delta)\Big\} + \theta_\alpha(k,\lambda)\phi_\alpha(k,\lambda)\{[K_\varepsilon(\xi,\zeta) + \\ & 2L_\varepsilon(\xi,\zeta)] + 3\phi_\alpha(k,\lambda)P_\varepsilon(\xi,\zeta)\Big\} + \theta_\alpha(k,\lambda)Q_\varepsilon(\xi,\zeta),\end{aligned} \tag{B.9}$$

$$\begin{aligned}R_\alpha(k,\lambda) = {} & \theta_\alpha^2(k,\lambda)\left[S_\beta(k,\delta) + R_\varepsilon(\xi,\zeta) - 1\right] \\ & + R_\beta(k,\delta) + 2\theta_\alpha(k,\lambda)U_\beta(k,\delta),\end{aligned} \tag{B.10}$$

$$\begin{aligned}S_\alpha(k,\lambda) = {} & \phi_\alpha^2(k,\lambda)\left[S_\beta(k,\delta) + R_\varepsilon(\xi,\zeta) - 1\right] \\ & + S_\varepsilon(\xi,\zeta) + 2\phi_\alpha(k,\lambda)U_\varepsilon(\xi,\zeta),\end{aligned} \tag{B.11}$$

$$\begin{aligned}U_\alpha(k,\lambda) = {} & \theta_\alpha(k,\lambda)\Big\{\phi_\alpha(k,\lambda)\left[S_\beta(k,\delta) + R_\varepsilon(\xi,\zeta) - 1\right] \\ & + U_\varepsilon(\xi,\zeta)\Big\} + R_\beta(k,\delta) + \phi_\alpha(k,\lambda)U_\beta(k,\delta),\end{aligned} \tag{B.12}$$

where θ_α and ϕ_α are given in Eq. (A.3) while the meaning of α, β, ε, δ, λ, ξ and ζ are specified in Table A1.

The initial conditions for the renormalization of PR are $I_F(0,1) = J_F(0,1) = 1$, $K_F(0,1) = L_F(0,1) = P_F(0,1) = Q_F(0,1) = 0$, $R_F(0,1) = S_F(0,1) = 1$, $U_F(0,1) = 0$, $E_L(0,1) = E_R(0,1) = 0$, $t_F(0,1) = t_B$, $I_F(1,1) = J_F(1,1) = 1$, $K_F(1,1) = L_F(1,1) = P_F(1,1) = Q_F(1,1) = 0$, $R_F(1,1) = S_F(1,1) = 1$, $U_F(1,1) = 0$, $E_L(1,1) = E_R(1,1) = 0$, and $t_F(1,1) = t_A$.

Appendix C. Renormalization formulas for the Kubo-Greenwood conductivity

In this article, the electrical conductivity (σ) is analyzed by means of the Kubo-Greenwood formula given by Eq. (19), in which the trace can be written as [30]

$$\begin{aligned}& Tr\{p\,\mathrm{Im}G^+(E+\hbar\omega)\,p\,\mathrm{Im}G^+(E)\} \\ & = \frac{m^2a^2}{4\hbar^2}\left[S(E_\omega^+, E^+, l) + S(E_\omega^-, E^-, l) - S(E_\omega^+, E^-, l) - S(E_\omega^-, E^+, l)\right]\end{aligned} \tag{C.1}$$

where $E_\omega^\pm = E + \hbar\omega \pm i\eta$, $E^\pm = E \pm i\eta$, η is the imaginary part of the energy and

$$\begin{aligned}& S(E_\omega^\kappa, E^\nu, l) \\ & = \sum_{i,j=1}^{N(l)-1} t_{i,i+1}t_{j,j+1}\Big\{2G_{i+1,j}^\kappa(E_\omega)G_{j+1,i}^\nu(E) \\ & - G_{i+1,j+1}^\kappa(E_\omega)G_{j,i}^\nu(E) - G_{i,j}^\kappa(E_\omega)G_{j+1,i+1}^\nu(E)\Big\},\end{aligned} \tag{C.2}$$

in which κ and ν could be $+$ or $-$. The partial sums $S(E_\omega^\kappa, E^\nu, l)$ can be written in terms of the Green's function at extreme sites of the system as

$$\begin{aligned}& S(E_\omega^\kappa, E^\nu, l) = Z_F(E_\omega^\kappa, E^\nu, l, 1) \\ & + A_F(E_\omega^\kappa, E^\nu, l, 1)G_{L,L}(E_\omega^\kappa)G_{L,L}(E^\nu) \\ & + B_F(E_\omega^\kappa, E^\nu, l, 1)G_{L,R}(E_\omega^\kappa)G_{L,R}(E^\nu) \\ & + C_F(E_\omega^\kappa, E^\nu, l, 1)G_{R,R}(E_\omega^\kappa)G_{R,R}(E^\nu) \\ & + D_F(E_\omega^\kappa, E^\nu, l, 1)G_{L,L}(E_\omega^\kappa)G_{L,R}(E^\nu) \\ & + D_F(E^\nu, E_\omega^\kappa, l, 1)G_{L,L}(E^\nu)G_{L,R}(E_\omega^\kappa) \\ & + F_F(E_\omega^\kappa, E^\nu, l, 1)G_{L,L}(E_\omega^\kappa)G_{R,R}(E^\nu) \\ & + F_F(E^\nu, E_\omega^\kappa, l, 1)G_{L,L}(E^\nu)G_{R,R}(E_\omega^\kappa) \\ & + I_F(E_\omega^\kappa, E^\nu, l, 1)G_{L,R}(E_\omega^\kappa)G_{R,R}(E^\nu) \\ & + I_F(E^\nu, E_\omega^\kappa, l, 1)G_{L,R}(E^\nu)G_{R,R}(E_\omega^\kappa) \\ & + J_F(E_\omega^\kappa, E^\nu, l, 1)G_{L,L}(E_\omega^\kappa) \\ & + J_F(E^\nu, E_\omega^\kappa, l, 1)G_{L,L}(E^\nu) \\ & + K_F(E_\omega^\kappa, E^\nu, l, 1)G_{L,R}(E_\omega^\kappa) \\ & + K_F(E^\nu, E_\omega^\kappa, l, 1)G_{L,R}(E^\nu) \\ & + L_F(E_\omega^\kappa, E^\nu, l, 1)G_{R,R}(E_\omega^\kappa) \\ & + L_F(E^\nu, E_\omega^\kappa, l, 1)G_{R,R}(E^\nu),\end{aligned} \tag{C.3}$$

where the subscripts L and R of the Green's function respectively denote the left and right extreme atom. The coefficients $A_F(E_1,E_2,l,1)$, $B_F(E_1,E_2,l,1)$, $\cdots$, $Z_F(E_1,E_2,l,1)$ in Eq. (C.3), being E_1 and E_2 either E_ω^κ or E^ν, can be iteratively calculated for $k = 2, 3, \cdots, l$ by means of

$$A_\alpha(E_1,E_2,k,\lambda) = -[P_\alpha(E_1,E_2,k,\lambda) - P_\alpha(E_2,E_1,k,\lambda)]^2, \tag{C.4}$$

$$\begin{aligned}B_\alpha(E_1,E_2,k,\lambda) = {} & 2[P_\alpha(E_1,E_2,k,\lambda) - \\ & P_\alpha(E_2,E_1,k,\lambda)][Q_\alpha(E_2,E_1,k,\lambda) - Q_\alpha(E_1,E_2,k,\lambda)] \\ & + 2[R_\alpha(E_1,E_2,k,\lambda) - S_\alpha(E_2,E_1,k,\lambda)]\times \\ & [R_\alpha(E_2,E_1,k,\lambda) - S_\alpha(E_1,E_2,k,\lambda)],\end{aligned} \tag{C.5}$$

$$C_\alpha(E_1,E_2,k,\lambda) = -[Q_\alpha(E_1,E_2,k,\lambda) - Q_\alpha(E_2,E_1,k,\lambda)]^2, \tag{C.6}$$

$$D_\alpha(E_1,E_2,k,\lambda) = 2[P_\alpha(E_1,E_2,k,\lambda)-P_\alpha(E_2,E_1,k,\lambda)] \times[S_\alpha(E_2,E_1,k,\lambda)-R_\alpha(E_1,E_2,k,\lambda)], \tag{C.7}$$

$$F_\alpha(E_1,E_2,k,\lambda) = -[R_\alpha(E_1,E_2,k,\lambda)-S_\alpha(E_2,E_1,k,\lambda)]^2, \tag{C.8}$$

$$I_\alpha(E_1,E_2,k,\lambda) = 2[Q_\alpha(E_1,E_2,k,\lambda)-Q_\alpha(E_2,E_1,k,\lambda)] \times[S_\alpha(E_2,E_1,k,\lambda)-R_\alpha(E_1,E_2,k,\lambda)], \tag{C.9}$$

$$\begin{aligned} J_\alpha(E_1,E_2,k,\lambda) &= \rho_\alpha(E_2,k,\lambda)F_\beta(E_1,E_2,k,\delta) \\ &+\theta_\alpha(E_1,k,\lambda)K_\beta(E_1,E_2,k,\delta)+\theta_\alpha(E_1,k,\lambda) \\ &\times\rho_\alpha(E_2,k,\lambda)\{I_\beta(E_1,E_2,k,\delta)+U_\alpha(E_1,E_2,k,\lambda) \\ &+\theta_\alpha(E_1,k,\lambda)[C_\beta(E_1,E_2,k,\delta)+A_\varepsilon(E_1,E_2,\xi,\zeta) \\ &+T_\alpha(E_1,E_2,k,\lambda)]\}+\theta_\alpha^2(E_1,k,\lambda) \\ &\times[L_\beta(E_1,E_2,k,\delta)+J_\varepsilon(E_1,E_2,\xi,\zeta)] \\ &+J_\beta(E_1,E_2,k,\delta), \end{aligned} \tag{C.10}$$

$$\begin{aligned} K_\alpha(E_1,E_2,k,\lambda) &= 2\rho_\alpha(E_2,k,\lambda)\theta_\alpha(E_1,k,\lambda) \\ &\times\phi_\alpha(E_1,k,\lambda)[C_\beta(E_1,E_2,k,\delta)+A_\varepsilon(E_1,E_2,\xi,\zeta) \\ &+T_\alpha(E_1,E_2,k,\lambda)]+\rho_\alpha(E_2,k,\lambda)V_\alpha(E_1,E_2,k,\lambda) \\ &+2\theta_\alpha(E_1,k,\lambda)\phi_\alpha(E_1,k,\lambda)[L_\beta(E_1,E_2,k,\delta) \\ &+J_\varepsilon(E_1,E_2,\xi,\zeta)]+\rho_\alpha(E_2,k,\lambda)\{\theta_\alpha(E_1,k,\lambda) \\ &\times[D_\varepsilon(E_2,E_1,\xi,\zeta)+W_\alpha(E_2,E_1,k,\lambda)]+ \\ &\phi_\alpha(E_1,k,\lambda)[I_\beta(E_1,E_2,k,\delta)+U_\alpha(E_1,E_2,k,\lambda)]\} \\ &+\phi_\alpha(E_1,k,\lambda)K_\beta(E_1,E_2,k,\delta) \\ &+\theta_\alpha(E_1,k,\lambda)K_\varepsilon(E_1,E_2,\xi,\zeta), \end{aligned} \tag{C.11}$$

$$\begin{aligned} L_\alpha(E_1,E_2,k,\lambda) &= \rho_\alpha(E_2,k,\lambda)F_\varepsilon(E_2,E_1,\xi,\zeta) \\ &+\phi_\alpha(E_1,k,\lambda)K_\varepsilon(E_1,E_2,\xi,\zeta)+\rho_\alpha(E_2,k,\lambda)\times \\ &\phi_\alpha(E_1,k,\lambda)\{D_\varepsilon(E_2,E_1,\xi,\zeta)+W_\alpha(E_2,E_1,k,\lambda) \\ &+\phi_\alpha(E_1,k,\lambda)[C_\beta(E_1,E_2,k,\delta)+A_\varepsilon(E_1,E_2,\xi,\zeta)+ \\ &T_\alpha(E_1,E_2,k,\lambda)]\}+\phi_\alpha^2(E_1,k,\lambda)[L_\beta(E_1,E_2,k,\delta) \\ &+J_\varepsilon(E_1,E_2,\xi,\zeta)]+L_\varepsilon(E_1,E_2,\xi,\zeta), \end{aligned} \tag{C.12}$$

and

$$\begin{aligned} Z_\alpha(E_1,E_2,k,\lambda) &= \rho_\alpha(E_1,k,\lambda)[L_\beta(E_1,E_2,k,\delta) \\ &+J_\varepsilon(E_1,E_2,\xi,\zeta)]+Z_\beta(E_1,E_2,k,\delta)+\rho_\alpha(E_1,k,\lambda) \\ &\times\rho_\alpha(E_2,k,\lambda)[C_\beta(E_1,E_2,k,\delta)+A_\varepsilon(E_1,E_2,\xi,\zeta) \\ &+T_\alpha(E_1,E_2,k,\lambda)]+\rho_\alpha(E_2,k,\lambda) \\ &\times[L_\beta(E_2,E_1,k,\delta)+J_\varepsilon(E_2,E_1,\xi,\zeta)] \\ &+Z_\varepsilon(E_1,E_2,\xi,\zeta), \end{aligned} \tag{C.13}$$

where the meaning of α, β, ε, δ, λ, ξ and ζ are specified in Table A1 for each stage of renormalization,

$$\rho_\alpha(E_\varphi,k,\lambda) = [z-E_L(E_\varphi,\xi,\zeta)-E_R(E_\varphi,k,\delta)]^{-1}, \tag{C.14}$$

$$\theta_\alpha(E_\varphi,k,\lambda) = t_\beta(E_\varphi,k,\delta)\rho_\alpha(E_\varphi,k,\lambda), \tag{C.15}$$

$$\phi_\alpha(E_\varphi,k,\lambda) = t_\varepsilon(E_\varphi,\xi,\zeta)\rho_\alpha(E_\varphi,k,\lambda), \tag{C.16}$$

$$E_L(E_\varphi,k,\lambda) = E_L(E_\varphi,k,\delta)+t_\beta^2(E_\varphi,k,\delta)\rho_\alpha(E_\varphi,k,\lambda), \tag{C.17}$$

$$E_R(E_\varphi,k,\lambda) = E_\varepsilon(E_\varphi,\xi,\zeta)+t_\varepsilon^2(E_\varphi,\xi,\zeta)\rho_\alpha(E_\varphi,k,\lambda), \tag{C.18}$$

$$t_\alpha(E_\varphi,k,\lambda) = t_\beta(E_\varphi,k,\delta)t_\varepsilon(E_\varphi,\xi,\zeta)\rho_\alpha(E_\varphi,k,\lambda), \tag{C.19}$$

$$\begin{aligned} P_\alpha(E_1,E_2,k,\lambda) &= \theta_\alpha(E_2,k,\lambda)R_\beta(E_1,E_2,k,\delta) \\ &+\theta_\alpha(E_1,k,\lambda)S_\beta(E_1,E_2,k,\delta)+\theta_\alpha(E_1,k,\lambda)\times \\ &\theta_\alpha(E_2,k,\lambda)[P_\varepsilon(E_1,E_2,\xi,\zeta)+Q_\beta(E_1,E_2,k,\delta)] \\ &+P_\beta(E_1,E_2,k,\delta), \end{aligned} \tag{C.20}$$

$$\begin{aligned} Q_\alpha(E_1,E_2,k,\lambda) &= \phi_\alpha(E_1,k,\lambda)R_\varepsilon(E_1,E_2,\xi,\zeta) \\ &+Q_\varepsilon(E_1,E_2,\xi,\zeta)+\phi_\alpha(E_2,k,\lambda)S_\varepsilon(E_1,E_2,\xi,\zeta) \\ &+\phi_\alpha(E_1,k,\lambda)\phi_\alpha(E_2,k,\lambda)[P_\varepsilon(E_1,E_2,\xi,\zeta) \\ &+Q_\beta(E_1,E_2,k,\delta)], \end{aligned} \tag{C.21}$$

$$\begin{aligned} R_\alpha(E_1,E_2,k,\lambda) &= \phi_\alpha(E_2,k,\lambda)R_\beta(E_1,E_2,k,\delta) \\ &+\theta_\alpha(E_1,k,\lambda)\phi_\alpha(E_2,k,\lambda)[P_\varepsilon(E_1,E_2,\xi,\zeta)+ \\ &Q_\beta(E_1,E_2,k,\delta)]+\theta_\alpha(E_1,k,\lambda)R_\varepsilon(E_1,E_2,\xi,\zeta), \end{aligned} \tag{C.22}$$

$$\begin{aligned} S_\alpha(E_1,E_2,k,\lambda) &= \phi_\alpha(E_1,k,\lambda)S_\beta(E_1,E_2,k,\delta) \\ &+\theta_\alpha(E_2,k,\lambda)\phi_\alpha(E_1,k,\lambda)[P_\varepsilon(E_1,E_2,\xi,\zeta)+ \\ &Q_\beta(E_1,E_2,k,\delta)]+\theta_\alpha(E_2,k,\lambda)S_\varepsilon(E_1,E_2,\xi,\zeta), \end{aligned} \tag{C.23}$$

$$T_\alpha(E_1,E_2,k,\lambda) = 2[P_\varepsilon(E_1,E_2,\xi,\zeta)-P_\varepsilon(E_2,E_1,\xi,\zeta)] \times[Q_\beta(E_2,E_1,k,\delta)-Q_\beta(E_1,E_2,k,\delta)], \tag{C.24}$$

$$U_\alpha(E_1,E_2,k,\lambda) = 2[P_\varepsilon(E_1,E_2,\xi,\zeta)-P_\varepsilon(E_2,E_1,\xi,\zeta)] \times[S_\beta(E_2,E_1,k,\delta)-R_\beta(E_1,E_2,k,\delta)], \tag{C.25}$$

$$V_\alpha(E_1,E_2,k,\lambda) = 2[S_\varepsilon(E_1,E_2,\xi,\zeta)-R_\varepsilon(E_2,E_1,\xi,\zeta)] \times[S_\beta(E_2,E_1,k,\delta)-R_\beta(E_1,E_2,k,\delta)], \tag{C.26}$$

and

$$W_\alpha(E_1,E_2,k,\lambda) = 2[Q_\beta(E_1,E_2,k,\delta)-Q_\beta(E_2,E_1,k,\delta)] \times[S_\varepsilon(E_2,E_1,\xi,\zeta)-R_\varepsilon(E_1,E_2,\xi,\zeta)], \tag{C.27}$$

being E_φ either E_1 or E_2.

The Green's functions at the ends of system are the same as in Appendix A, except they are evaluated at E_φ instead of z, *i.e.*,

$$G_{L,L}(E_\varphi) = \left\{E_\varphi-E_L(E_\varphi,l,1)-\frac{t_P^2(l')}{E_\varphi-E_P^L(l')} -E_P^R(l')-\frac{t_F^2(E_\varphi,l,1)}{E_\varphi-E_R(E_\varphi,l,1)-E_P^L(l')-\frac{t_P^2(l')}{E_\varphi-E_P^R(l')}}\right\}^{-1}, \tag{C.28}$$

$$G_{R,R}(E_\varphi) = \left\{E_\varphi-E_R(E_\varphi,l,1)-\frac{t_P^2(l')}{E_\varphi-E_P^R(l')} -E_P^L(l')-\frac{t_F^2(E_\varphi,l,1)}{E_\varphi-E_L(E_\varphi,l,1)-E_P^R(l')-\frac{t_P^2(l')}{E_\varphi-E_P^L(l')}}\right\}^{-1}, \tag{C.29}$$

and

$$G_{L,R}(E_\varphi) = \frac{t_F(E_\varphi,l,1)G_{R,R}(E_\varphi)}{E_\varphi-E_L(E_\varphi,l,1)-E_P^R(l')-\frac{t_P^2(l')}{E_\varphi-E_P^L(l')}}. \tag{C.30}$$

Finally, the initial conditions are $A_F(E_1,E_2,0,1)=0$, $C_F(E_1,E_2,0,1)=0$, $D_F(E_1,E_2,0,1)=0$, $I_F(E_1,E_2,0,1)=0$, $J_F(E_1,E_2,0,1)=0$, $K_F(E_1,E_2,0,1)=0$, $L_F(E_1,E_2,0,1)=0$, $Z_F(E_1,E_2,0,1)=0$, $P_F(E_1,E_2,0,1)=0$, $Q_F(E_1,E_2,0,1)=0$, $R_F(E_1,E_2,0,1)=0$, $E_L(E_\varphi,0,1)=0$, $E_R(E_\varphi,0,1)=0$, $B_F(E_1,E_2,0,1)=2t_B^2$, $F_F(E_1,E_2,0,1)=-t_B^2$, $t_F(E_\varphi,0,1)=t_B$, $A_F(E_1,E_2,1,1)=0$, $S_F(E_1,E_2,0,1)=t_B$, $C_F(E_1,E_2,1,1)=0$, $D_F(E_1,E_2,1,1)=0$, $I_F(E_1,E_2,1,1)=0$, $J_F(E_1,E_2,1,1)=0$, $K_F(E_1,E_2,1,1)=0$, $L_F(E_1,E_2,1,1)=0$, $Z_F(E_1,E_2,1,1)=0$, $P_F(E_1,E_2,1,1)=0$, $Q_F(E_1,E_2,1,1)=0$, $R_F(E_1,E_2,1,1)=0$, $E_L(E_\varphi,1,1)=0$, $E_R(E_\varphi,1,1)=0$, $B_F(E_1,E_2,1,1)=2t_A^2$, $F_F(E_1,E_2,1,1)=-t_A^2$, $S_F(E_1,E_2,1,1)=t_A$, and $t_F(E_\varphi,1,1)=t_A$.

References

[1] E. Abrahams, P.W. Anderson, D.C. Licciardello, T.V. Ramakrishnan, Phys. Rev. Lett. 42 (1979) 673.
[2] C. Flores, J. Phys. C 1 (1989) 8471.
[3] D.H. Dunlap, H.L. Wu, P.W. Phillips, Phys. Rev. Lett. 65 (1990) 88.

[4] V. Bellani, E. Diez, R. Hey, L. Toni, L. Tarricone, G.B. Parravicini, F. Domínguez-Adame, R. Gómez-Alcalá, Phys. Rev. Lett. 82 (1999) 2159.
[5] U. Kuhl, F.M. Izrailev, A.A. Krokhin, H.J. Stöckmann, Appl. Phys. Lett. 77 (2000) 633.
[6] D. Shechtman, I. Blech, D. Gratias, J.W. Cahn, Phys. Rev. Lett. 53 (1984) 1951.
[7] R. Merlin, K. Bajema, R. Clarke, F.Y. Juang, P.K. Bhattacharya, Phys. Rev. Lett. 55 (1985) 1768.
[8] C. Wang, R.A. Barrio, Phys. Rev. Lett. 61 (1988) 191.
[9] M. Kohmoto, B. Sutherland, C. Tang, Phys. Rev. B 35 (1987) 1020.
[10] A. Sütő, J. Stat. Phys. 56 (1989) 525.
[11] E. Maciá, Rep. Prog. Phys. 75 (2012) 036502.
[12] G. Gumbs, M.K. Ali, Phys. Rev. Lett. 60 (1988) 1081.
[13] G. Gumbs, G.S. Dubey, A. Salman, B.S. Mahmoud, D. Huang, Phys. Rev. B 52 (1995) 210.
[14] A.G. Barriuso, J.J. Monzón, T. Yonte, A. Felipe, L.L. Sánchez-Soto, Opt. Express 21 (2013) 30039.
[15] J.X. Zhong, J.R. Yan, J.Q. You, J. Phys. A Math. Gen. 24 (1991) L949.
[16] A. Chakrabarti, S.N. Karmakar, Phys. Rev. B 44 (1991) 896.
[17] V. Sánchez, L.A. Pérez, R. Oviedo-Roa, C. Wang, Phys. Rev. B 64 (2001) 174205.
[18] V. Sanchez, C. Wang, J. Alloys Compd. 342 (2002) 410.
[19] V. Sánchez, C. Wang, Philos. Mag. 95 (2015) 326.
[20] G.Y. Oh, M.H. Lee, Phys. Rev. B 48 (1993) 12465.
[21] X. Fu, Y. Liu, Z. Gou, P. Zhou, X. Huang, Phys. Rev. B 51 (1995) 3910.
[22] E. Maciá, Aperiodic Structures in Condensed Matter: Fundamentals and Applications, CRC Press, Boca Raton, 2009 132.
[23] J.W.S. Cassels, An Introduction to Diophantine Approximation, Cambridge University Press, Cambridge, 1957 133.
[24] J.M. Luck, C. Godreche, A. Janner, T. Janssen, J. Phys. A Math. Gen. 26 (1993) 1951.
[25] W. Steurer, Crytallography of Quasicrystals, Springer, Berlin, 2009 13.
[26] E.N. Economou, Green's Functions in Quantum Physics, Springer, Berlin, 2006 7.
[27] R. Oviedo-Roa, L.A. Pérez, C. Wang, Phys. Rev. B 62 (2000) 13805.
[28] Y. Imry, R. Landauer, Rev. Mod. Phys. 71 (1999) S306.
[29] B. Kramer, A. MacKinon, Rep. Prog. Phys. 56 (1993) 1469.
[30] V. Sánchez, C. Wang, Phys. Rev. B 70 (2004) 144207.
[31] S. Thiem, M. Schreiber, Eur. Phys. J. B 83 (2011) 415.
[32] V. Sánchez, C. Wang, Int. J. Comp. Mat. Sci. Eng. 1 (2012) 1250003.
[33] D. Damanik, Lett. Math. Phys. 46 (1998) 303.
[34] C. Wang, C. Ramírez, F. Sánchez, V. Sánchez, Phys. Status Solidi B 252 (2015) 1370.